# Replication stress promotes cell elimination by extrusion

https://doi.org/10.1038/s41586-021-03526-y

Received: 26 December 2019

Accepted: 9 April 2021

Published online: 05 May 2021

Check for updates

Vivek K. Dwivedi[1], Carlos Pardo-Pastor[2], Rita Droste[1], Ji Na Kong[1], Nolan Tucker[1], Daniel P. Denning[1,3], Jody Rosenblatt[2] & H. Robert Horvitz[1]✉

Cell extrusion is a mechanism of cell elimination that is used by organisms as diverse as sponges, nematodes, insects and mammals[1–3]. During extrusion, a cell detaches from a layer of surrounding cells while maintaining the continuity of that layer[4]. Vertebrate epithelial tissues primarily eliminate cells by extrusion, and the dysregulation of cell extrusion has been linked to epithelial diseases, including cancer[1,5]. The mechanisms that drive cell extrusion remain incompletely understood. Here, to analyse cell extrusion by *Caenorhabditis elegans* embryos[3], we conducted a genome-wide RNA interference screen, identified multiple cell-cycle genes with S-phase-specific function, and performed live-imaging experiments to establish how those genes control extrusion. Extruding cells experience replication stress during S phase and activate a replication-stress response via homologues of ATR and CHK1. Preventing S-phase entry, inhibiting the replication-stress response, or allowing completion of the cell cycle blocked cell extrusion. Hydroxyurea-induced replication stress[6,7] triggered ATR–CHK1- and p53-dependent cell extrusion from a mammalian epithelial monolayer. We conclude that cell extrusion induced by replication stress is conserved among animals and propose that this extrusion process is a primordial mechanism of cell elimination with a tumour-suppressive function in mammals.

Mutants of *C. elegans* that are defective in caspase-mediated apoptosis—for example, *ced-3(lf)* loss-of-function mutants—provide an excellent system for studies of cell extrusion[3]. Cell extrusion functions as a 'backup' mechanism in *ced-3(lf)* embryos to eliminate certain cells that would normally be eliminated by caspase-mediated apoptosis[3]. To identify genes that control cell extrusion, we screened the *C. elegans* ORFeome RNA interference (RNAi) library of 11,511 bacterial clones for RNAi clones that in *ced-3(lf)* animals generated the two-excretory cell (Tex) phenotype[3] (Fig. 1a–c, Extended Data Fig. 1a), which occurs when the cell ABplpappap fails to be extruded. From this screen, we identified 30 RNAi clones corresponding to 27 genes that produced a Tex phenotype (Extended Data Fig. 1a). Notably, 10 of the 27 genes identified were cell-cycle genes with functions that were mostly specific to the S phase[8] (Fig. 1d, e). Additional RNAi screens identified an additional four such genes (Fig. 1d, Extended Data Table 1). Consistent with their function in cell extrusion, RNAi against 13 of the 14 identified cell-cycle genes produced a Tex phenotype only in the *ced-3(lf)* background and not in a *ced-3(+)* wild-type background (Extended Data Table 2).

## Cell-cycle genes promote cell extrusion

To characterize the functional role of cell-cycle genes in cell extrusion, we used time-lapse confocal microscopy to observe ABplpappap in embryos treated with RNAi against *cye-1* or *cdk-2* or with an empty vector (control embryos). We tracked the fate of ABplpappap over a 50-min period ending in ventral enclosure, which normally coincides with cell extrusion[3] (Fig. 1f, Extended Data Fig. 1b, Supplementary Videos 1–3). Virtual lateral sections of the embryos at the end of ventral enclosure confirmed that ABplpappap was extruded from control embryos (10 of 11 embryos) (Fig. 1g). By contrast, ABplpappap was not extruded from *cye-1(RNAi)* (11 of 11) (Fig. 1g) or *cdk-2(RNAi)* embryos (10 of 11) (Fig. 1g), consistent with the highly penetrant Tex phenotype observed for *cye-1(RNAi)* and *cdk-2(RNAi)* larval animals (Fig. 1d, e). We conclude that *cye-1* and *cdk-2* are required for extrusion of the cell ABplpappap.

To identify the cellular site of cell-cycle gene function in ABplpappap cell extrusion, we performed genetic mosaic analyses. We examined *cye-1(lf); ced-3(lf)* double mutants and found that these animals displayed a Tex phenotype similar to that of *ced-3(lf); cye-1(RNAi)* animals (Fig. 1d, h), suggesting that extrusion is more sensitive to a reduction in cell-cycle gene levels than general embryonic development, for which maternal contribution of *cye-1* is sufficient[9]. We generated an extrachromosomal array carrying the cell-autonomous RFP reporter $P_{sur\text{-}5}$*::RFP* and a *cye-1(+)* transgene, which partially rescued the Tex phenotype of *cye-1(lf); ced-3(lf)* animals (Fig. 1h). Extrachromosomal arrays are mitotically unstable and are randomly lost during development, which produces mosaic animals. We examined ten mosaic animals that carried the *cye-1(+)*-rescuing array, as indicated by the presence of RFP in any set of cells or tissues, but were not rescued for the Tex phenotype (Fig. 1i). The RFP expression pattern indicated that the array was absent from ABplpappap in all ten animals, despite being present in the ABplpappap niece cell (the excretory cell) in nine of the ten animals (Fig. 1i–k, Extended Data Fig. 2a–i). We conclude that *cye-1* and

[1]Howard Hughes Medical Institute, Department of Biology, Massachusetts Institute of Technology, Cambridge, MA, USA. [2]Randall Centre for Cell & Molecular Biophysics, King's College London, London, UK. [3]Novartis Institutes for BioMedical Research, Cambridge, MA, USA. ✉e-mail: horvitz@mit.edu

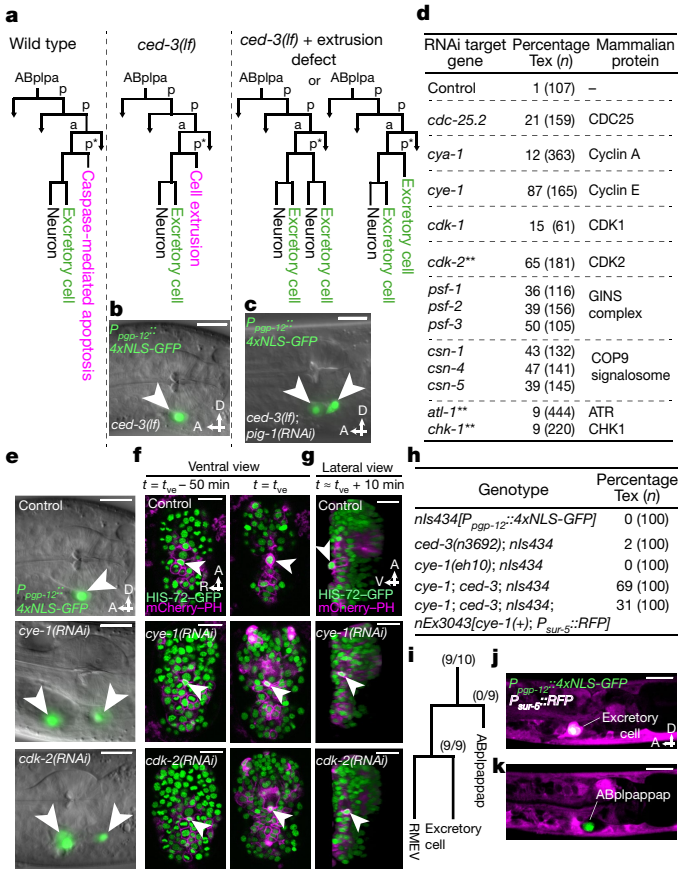


| RNAi target gene | Percentage Tex (*n*) | Mammalian protein |
|---|---|---|
| Control | 1 (107) | – |
| *cdc-25.2* | 21 (159) | CDC25 |
| *cya-1* | 12 (363) | Cyclin A |
| *cye-1* | 87 (165) | Cyclin E |
| *cdk-1* | 15 (61) | CDK1 |
| *cdk-2*** | 65 (181) | CDK2 |
| *psf-1*<br>*psf-2*<br>*psf-3* | 36 (116)<br>39 (156)<br>50 (105) | GINS complex |
| *csn-1*<br>*csn-4*<br>*csn-5* | 43 (132)<br>47 (141)<br>39 (145) | COP9 signalosome |
| *atl-1*** | 9 (444) | ATR |
| *chk-1*** | 9 (220) | CHK1 |

| Genotype | Percentage Tex (*n*) |
|---|---|
| *nIs434[P<sub>pgp-12</sub>::4xNLS-GFP]* | 0 (100) |
| *ced-3(n3692); nIs434* | 2 (100) |
| *cye-1(eh10); nIs434* | 0 (100) |
| *cye-1; ced-3; nIs434* | 69 (100) |
| *cye-1; ced-3; nIs434; nEx3043[cye-1(+); P<sub>sur-5</sub>::RFP]* | 31 (100) |

**Fig. 1 | Cell-cycle genes control cell extrusion cell autonomously.** **a**, Sublineage diagram showing the fate of ABplpappap (asterisk) in wild-type and *ced-3(lf)* animals and in *ced-3(lf)* animals that also had a defect in extrusion. **b**, **c**, Merged epifluorescence and Nomarski micrographs of the pharyngeal region of *nIs433[P<sub>pgp-12</sub>::4×NLS-GFP]; ced-3(lf)* (**b**) and extrusion-defective *nIs433; ced-3(lf); pig-1(RNAi)* (**c**) animals[3]. **d**, The percentages of animals with the Tex phenotype in *ced-3(lf)* animals after the indicated RNAi treatment. **Identified from candidate RNAi screens; others identified from screen shown in Extended Data Fig. 1a. **e**, Merged epifluorescence and Nomarski micrographs of the pharyngeal region of *nIs433; ced-3(lf)* animals after the indicated RNAi treatment. **f**, **g**, Ventral and virtual lateral views of *ced-3(lf); stIs10026[his-72::GFP]; nIs632[P<sub>egl-1</sub>::mCherry::PH]* embryos after the indicated RNAi treatment at the indicated time point. $t_{ve}$, time point of ventral enclosure. **h**, Percentages of animals of the indicated genotypes with the Tex phenotype. **i**, Cell-lineage diagram showing the number of animals with the Tex phenotype carrying the *cye-1(+)*-rescuing array *nEx3043* in the indicated lineage or cell in ten *cye-1(lf); ced-3(lf); nIs434[P<sub>pgp-12</sub>::4xNLS-GFP]* animals. **j**, **k**, Two confocal fluorescence micrographs of one of ten *cye-1(lf); ced-3(lf); nIs434; nEx3043* genetic mosaic worms represented in **i**. Arrowheads, excretory or ectopic excretory-like cells in **b**, **c**, **e**; ABplpappap in **f**, **g**. A, anterior; D, dorsal; R, right; V, ventral. Scale bars, 10 µm.

probably other cell-cycle genes function cell-autonomously for the extrusion of ABplpappap.

## Cells arrest in S phase before extrusion

To characterize the cell-cycle phase of cells that are extruded, we used two cell-cycle reporters: (i) tDHB–GFP[10], a truncated DNA helicase B fragment fused to GFP, and (ii) GFP–PCN-1, an N-terminal translational fusion of GFP to the *C. elegans* homologue of the DNA replication processivity factor PCNA[11]. tDHB–GFP is enriched in the nuclei of quiescent, post-mitotic and G1-phase cells and transits to the cytoplasm for all other cell-cycle phases[10] (Fig. 2a); GFP–PCN-1 exhibits a punctate

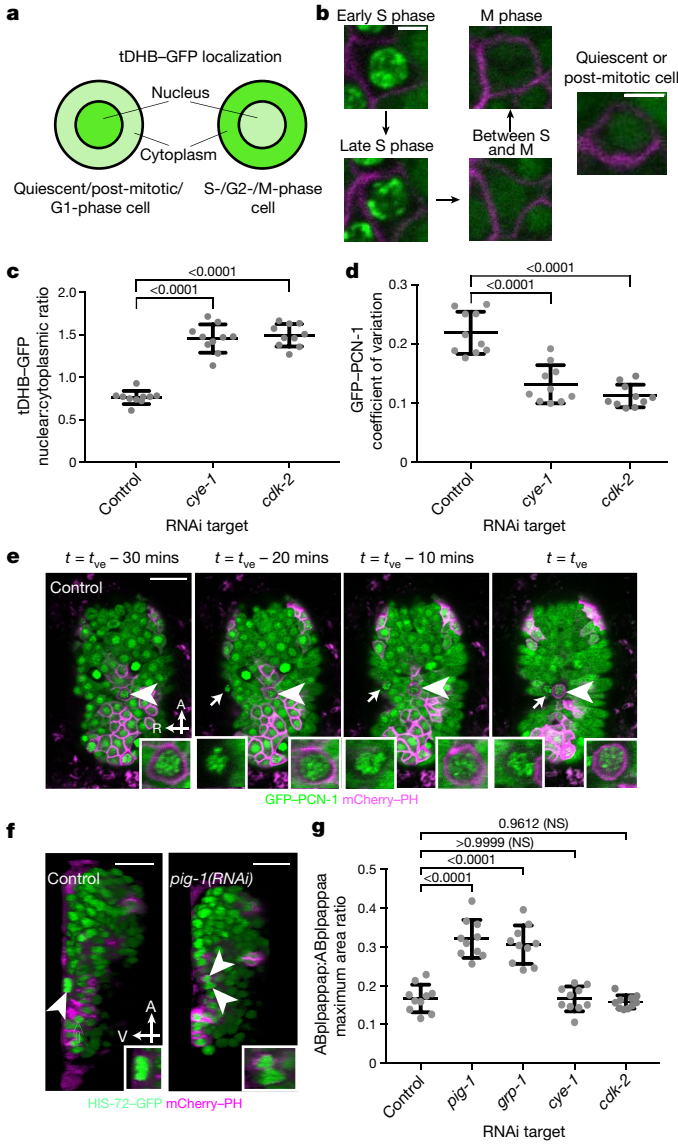


**Fig. 2 | Cells undergoing extrusion arrest in S phase.** **a**, Relative nuclear and cytoplasmic localization of a tDHB–GFP fusion protein in the indicated cell-cycle phases[10]. **b**, Localization pattern of GFP–PCN-1 in a typical *C. elegans* embryonic cell in the indicated cell-cycle phase. **c**, Nuclear:cytoplasmic ratio of tDHB–GFP fluorescence intensity in ABplpappap in *heSi192[P<sub>eft-3</sub>::tDHB-GFP]; ced-3(lf); nIs861[P<sub>egl-1</sub>::mCherry::PH]* embryos after the indicated RNAi treatment. **d**, Quantification of the coefficient of variation of GFP–PCN-1 fluorescence intensity in *ced-3(lf); isIs17[P<sub>pie-1</sub>::GFP::pcn-1]; nIs861* embryos after indicated RNAi treatment. **e**, Time-lapse confocal fluorescence micrographs of GFP–PCN-1 fluorescence in ABplpappap (arrowhead and right insets) in *ced-3(lf); isIs17; nIs861* embryos at the indicated times after treatment with control RNAi. Arrow, unidentified extruding cell (left insets). **f**, Micrographs of virtual lateral section of *ced-3(lf); nIs861; stIs10026[his-72::GFP]* embryos showing either ABplpappap (left, arrowhead) or its daughter cells (right, arrowheads) after indicated RNAi treatment. **g**, Quantification of the ratio of the maximum area occupied by ABplpappap to that occupied by its sister cell, ABplpappaa, in *ced-3(lf); ltIs44[P<sub>pie-1</sub>::mCherry::PH]; stIs10026* embryos after the indicated RNAi treatment. Insets, magnified view of ABplpappap or its daughter cells. Scale bars, 2 µm (**b**); 10 µm (all other micrographs). **c**, **d**, **g**, $n = 10$ embryos (biological replicates) for each RNAi treatment; mean ± s.d.; ordinary one-way ANOVA with Dunnett's correction for multiple comparisons. *P* values are indicated; NS, not significant.

sub-nuclear localization only during S phase in both mammalian and early *C. elegans* embryonic cells[11,12] (Fig. 2b). In control embryos, tDHB–GFP reporter fluorescence was mostly absent from the ABplpappap

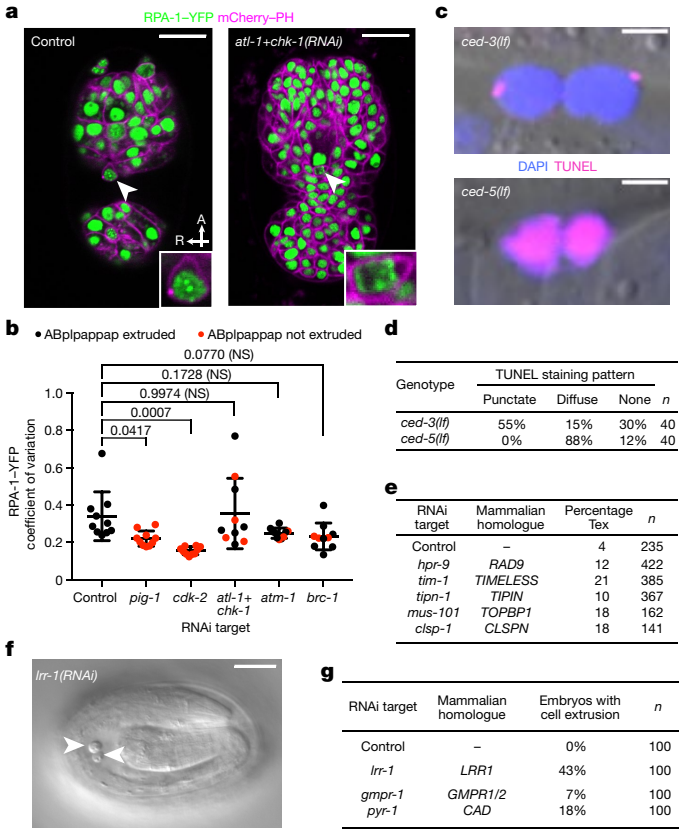


| Genotype | TUNEL staining pattern | | | |
|---|---|---|---|---|
| | Punctate | Diffuse | None | *n* |
| *ced-3(lf)* | 55% | 15% | 30% | 40 |
| *ced-5(lf)* | 0% | 88% | 12% | 40 |

| RNAi target | Mammalian homologue | Percentage Tex | *n* |
|---|---|---|---|
| Control | – | 4 | 235 |
| *hpr-9* | *RAD9* | 12 | 422 |
| *tim-1* | *TIMELESS* | 21 | 385 |
| *tipn-1* | *TIPIN* | 10 | 367 |
| *mus-101* | *TOPBP1* | 18 | 162 |
| *clsp-1* | *CLSPN* | 18 | 141 |

| RNAi target | Mammalian homologue | Embryos with cell extrusion | *n* |
|---|---|---|---|
| Control | – | 0% | 100 |
| *lrr-1* | *LRR1* | 43% | 100 |
| *gmpr-1* | *GMPR1/2* | 7% | 100 |
| *pyr-1* | *CAD* | 18% | 100 |

**Fig. 3 | Replication stress is coincident with and promotes cell extrusion.** **a**, Confocal fluorescence micrographs showing the localization of RPA-1–YFP in ABplpappap (arrowhead) in *ced-3(lf); ltIs44; opIs263[$P_{rpa\text{-}1}$::rpa-1::YFP]* embryos after the indicated RNAi treatment. Inset, magnified view of ABplpappap. Scale bars, 10 µm. **b**, Coefficient of variation of RPA-1–YFP fluorescence intensity in ABplpappap in *ced-3(lf); ltIs44; opIs263* embryos after the indicated RNAi treatments. $n = 10$ embryos (biological replicates) for each RNAi treatment; mean ± s.d.; *P* values shown for ordinary one-way ANOVA with Dunnett's correction for multiple comparison; NS, not significant. **c**, Merged Nomarski and fluorescence micrographs showing DAPI and TUNEL staining in extruded cells in embryos of indicated genotype. Scale bars, 2 µm. **d**, Percentage of observed extruded cells in embryos of the indicated genotypes with the indicated TUNEL staining pattern. **e**, Percentages of *ced-3(lf)* animals with the Tex phenotype after the indicated RNAi treatment along with mammalian homologues of the RNAi targets. **f**, Nomarski micrograph showing cells extruded (arrowheads) from wild-type embryos after *lrr-1(RNAi)*. Scale bar, 10 µm. **g**, Percentages of wild-type embryos exhibiting cell extrusion after the indicated RNAi treatments along with mammalian homologues of RNAi targets.

nucleus (Fig. 2c) both before ventral enclosure (five of five embryos) (Extended Data Fig. 3a) and after extrusion (five of five embryos) (Extended Data Fig. 3b). Cells extruded from other sites of control or untreated embryos also displayed low levels of nuclear tDHB–GFP (Extended Data Fig. 4a–d). Therefore, ABplpappap and other extruded cells appear to enter but never complete the cell cycle during extrusion.

The GFP–PCN-1 reporter localized to bright sub-nuclear punctate foci in ABplpappap cells (Fig. 2d) both before extrusion (five of five embryos) (Extended Data Fig. 3c) and after extrusion (five of five embryos) (Extended Data Fig. 3d) from control embryos, indicating that ABplpappap entered but did not exit S phase. Time-lapse confocal microscopy of an embryo progressing towards ventral enclosure confirmed that GFP–PCN-1 localization did not change in either ABplpappap or a second, unidentified extruding cell, indicating that S phase was arrested in both cells during the period that ended in their extrusion (Fig. 2e, Supplementary Video 4). Nearly all cells extruded from *ced-3(lf)* embryos displayed bright sub-nuclear foci of GFP–PCN-1 (Extended Data Fig. 4e, f). We conclude that cells extruded by *ced-3(lf)* embryos enter the cell cycle before extrusion, arrest in S phase, and are then extruded.

The treatment of embryos with RNAi against *cye-1* or *cdk-2* markedly altered the localization of tDHB–GFP and GFP–PCN-1 in ABplpappap. tDHB–GFP localized to the ABplpappap nucleus (Fig. 2c) and GFP–PCN-1 was diffusely nuclear in ABplpappap (Fig. 2d) in *cye-1(RNAi)* and *cdk-2(RNAi)* embryos both before (five of five embryos each) (Extended Data Fig. 3a, c) and after ventral enclosure (five of five embryos each) (Extended Data Fig. 3b, d). These observations show that ABplpappap fails to enter the cell cycle in embryos with reduced CYE-1 and CDK-2 and indicate that progression to S phase is required for cell extrusion.

Next we tested whether the previously identified cell-extrusion regulators[3] *pig-1* and *grp-1* also promote S-phase arrest. Unexpectedly, we found that ABplpappap in *pig-1(RNAi)* embryos completed the cell cycle and divided into daughter cells before ventral enclosure (Extended Data Fig. 3e, Supplementary Video 5); virtual lateral sections confirmed that the daughter cells were not extruded (five of six embryos) (Fig. 2f). ABplpappap similarly divided to generate surviving daughters in *grp-1(RNAi)* embryos (six of six embryos) (Extended Data Fig. 3f). Thus, failure either to initiate the cell cycle, as in *cye-1(RNAi)* or *cdk-2(RNAi)* embryos, or to arrest at S-phase, as in *pig-1(RNAi)* or *grp-1(RNAi)* embryos (Fig. 2f, Extended Data Fig. 3f–h), is associated with impaired cell extrusion.

Given that *pig-1* and *grp-1* regulate unequal cell divisions in multiple *C. elegans* cell lineages (for example, the QR/L neuroblast lineages[13]), we tested whether they control the unequal division of ABplpappa, which produces the extruded cell ABplpappap and a sister cell almost 2.5-fold larger in diameter (Fig. 2g, Extended Data Fig. 3i). Both *pig-1(RNAi)* and *grp-1(RNAi)* generated an abnormally large ABplpappap cell (Fig. 2g, Extended Data Fig. 3i–k); by contrast, RNAi against *cye-1* or *cdk-2* did not affect the highly unequal ABplpappa division (Fig. 2g, Extended Data Fig. 3i, l, m). Thus, unequal cell division precedes S-phase cell-cycle arrest in the small daughter cell that is fated for extrusion, whereas an abnormally large ABplpappap is competent to complete the cell cycle.

## Extruding cells show replication stress

We speculated that ABplpappap enters S-phase arrest because it inherits from the unequal ABplpappa division a pool of resources that is insufficient to support DNA replication. We therefore examined ABplpappap for evidence of replication stress using a reporter of RPA-1, the *C. elegans* homologue of mammalian replication protein A. RPA-1 binds in distinct nuclear foci to single-stranded DNA segments generated during replication stress[14]. We observed that an RPA-1–YFP fusion protein localized to a small number of distinct foci in ABplpappap in control embryos (Fig. 3a, b), indicating that this cell undergoes replication stress; other extruded cells exhibited a similar pattern of RPA-1–YFP foci (Extended Data Fig. 4g–j). By contrast, RPA-1–YFP was more diffuse in ABplpappap in *pig-1(RNAi)* or *cdk-2(RNAi)* embryos (Fig. 3b, Extended Data Fig. 5a, b), indicating, respectively, the absence of replication stress when ABplpappap is either abnormally large (with sufficient resources for DNA synthesis) or prevented from S-phase entry. In addition, most cells extruded from *ced-3(lf)* embryos displayed punctate TUNEL staining, indicative of limited DNA damage[15] (Fig. 3c, d) and unlike the diffuse staining of cells undergoing caspase-mediated apoptosis[16], such as those visible in *ced-5(lf)* embryos (Fig. 3c, d). This observation suggests that a replication-stress response might limit TUNEL-reactive DNA damage[17] in extruded cells. In short, cells extruded by *ced-3(lf)* embryos exhibited multiple hallmarks of replication stress.

To determine whether the replication-stress response directly promotes cell extrusion, we treated *ced-3(lf)* animals with RNAi against genes that encode critical replication-stress response proteins: TopBP1 (*mus-101*), Claspin (*clsp-1*), Timeless (*tim-1*), Tipin (*tipn-1*), Rad9 (*hpr-9*), ATR (*atl-1*) and CHK1 (*chk-1*)[18]. These RNAi

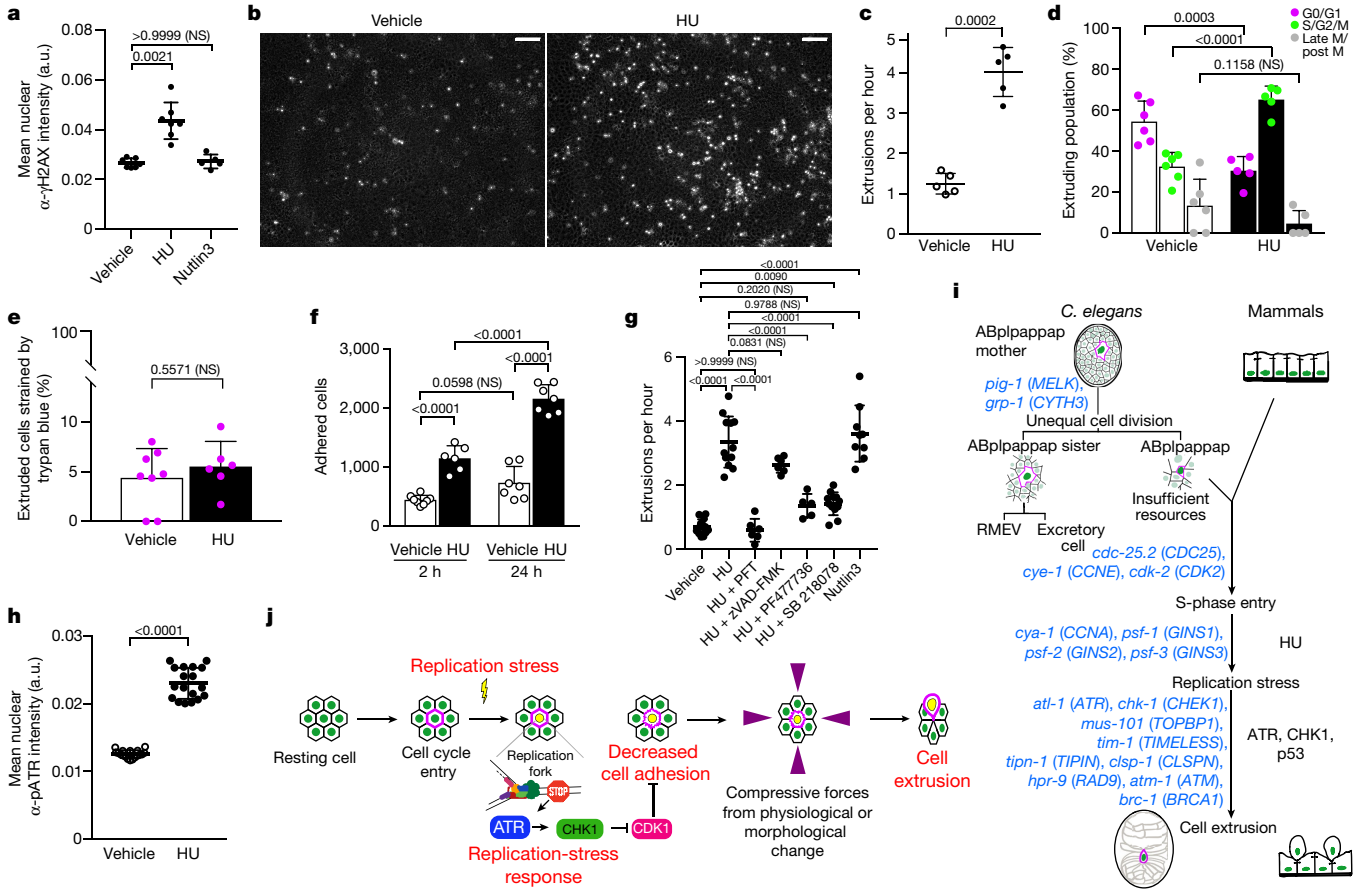


**Fig. 4 | Replication stress promotes cell extrusion from a simple mammalian epithelial layer. a**, Quantification of anti-γH2AX immunofluorescence signal in MDCK-II cells treated with vehicle, HU, or Nutlin-3. **b**, Representative micrographs of cells extruded (white rounded spots) from an MDCK-II monolayer after about 21 h of treatment with vehicle control (left) or HU (right). Scale bars, 100 μm. **c**, **g**, Quantification of extrusions per hour after the indicated treatments. **d**, The cell-cycle phases of cells extruded after treatment with vehicle control or HU. **e**, Percentage of extruded cells that stained with trypan blue after indicated treatments. **f**, The number of HU-treated or vehicle-treated extruded cells that adhered at 2 h and 24 h after reseeding in fresh medium. **h**, Quantification of anti-pATR immunofluorescence signal in vehicle- or HU-treated MDCK-II cells. **i**,**j**, Summary and model of replication-stress induced cell extrusion. Each data point, separate experiment in **c**–**g**; mean fluorescence intensity signal from one image of hundreds of cells in **a**, **h**. $n = 7, 7$ and 5 for vehicle, HU and Nutlin3, respectively (**a**); 5 each (**c**); 6 for vehicle, 5 for HU (**d**); 8 for vehicle, 6 for HU (**e**); 8 for vehicle, 6 for HU at 2 h and 7 each at 24 h (**f**); 13, 12, 6, 6, 5, 12 and 9 for vehicle, HU, HU + PFT, HU + zVAD-FMK, HU + PF477736, HU + SB218078 and Nutlin-3, respectively (**g**); 18 each (**h**), all biologically independent. All data in **a**, **c**–**h** are represented as mean ± s.d. Statistical analysis: Kruskal–Wallis one-way ANOVA followed by Dunn's correction (**a**); two-tailed Welch's *t*-test (**c**); ordinary one-way ANOVA with Sidak's correction (**d**, **f**, **g**); Mann–Whitney two-tailed test (**e**, **h**). *P* values are indicated; NS, not significant.

treatments produced a Tex phenotype (Figs. 1d, 3e), indicating that the replication-stress response pathway is necessary for cell extrusion. Furthermore, RNAi against *atm-1* (*ATM* homologue), *brc-1* (*BRCA1* homologue), or both *atl-1* (*ATR* homologue) and *chk-1* (*CHEK1* homologue) prevented ABplpappap extrusion in three to four of the ten embryos examined after each treatment, despite the presence of RPA-1–YFP foci in the unextruded ABplpappap cell (Fig. 3a, b, Extended Data Fig. 5c, d). Thus, inhibition of the canonical replication-stress response signalling pathway prevented extrusion of cells undergoing replication stress.

We hypothesized that the source of replication stress in ABplpappap and other extruded cells is an insufficient pool of DNA replication proteins or nucleotides resulting from the unequal division of their mother cells (for example, ABplpappa). We noted that genes previously identified from a screen for suppression of *lrr-1(lf)*-induced sterility[19] also suppressed cell extrusion by *ced-3(lf)* animals (Extended Data Fig. 5e). *lrr-1* encodes an adaptor protein for the $CRL2^{LRR-1}$ E3 ubiquitin ligase and is required for the disassembly of terminated replisomes[20,21]. Loss of *lrr-1* produces abnormalities in mitotic germline cells similar to those we observed in cells extruded from *ced-3(lf)* embryos: activation of the ATL-1–CHK-1-dependent replication-stress response, S-phase arrest, and DNA damage[22]. In addition, we found that *lrr-1(RNAi)* caused ectopic extrusion of unidentified cells in a wild-type background (Fig. 3f, g). These findings indicate that LRR-1 insufficiency in the small ABplpappap cell can drive its extrusion from *ced-3(lf)* embryos, presumably by preventing the efficient removal of terminated replisomes. We also found that RNAi against a gene required for pyrimidine nucleotide synthesis (*pyr-1*) or a gene required for the maintenance of purine nucleotide balance (*gmpr-1*) similarly caused ectopic extrusion of unidentified cells in wild-type animals (Fig. 3g, Extended Data Fig. 5f). (The *C. elegans* gene *F32D1.5* is referred to here as *gmpr-1*. A request to change the name of *F32D1.5* to *gmpr-1* has been approved by WormBase and this change will be reflected in a future WormBase release.) *pyr-1* and *gmpr-1* encode the *C. elegans* homologues of mammalian CAD and GMP reductase enzymes, respectively. Thus, perturbation of nucleotide levels is sufficient to drive cell extrusion. We propose that low levels of LRR-1 combined with insufficient nucleotide pools can result in replication stress and S-phase arrest in, and ultimately cell extrusion of, the small daughter cells of unequal cell divisions.

## An evolutionarily conserved cell-extrusion mechanism

To test whether replication stress-mediated cell extrusion is an evolutionarily conserved process, we examined monolayers of Madin-Darby canine kidney (MDCK-II) cells treated with 2 mM hydroxyurea (HU) to induce replication stress[6,7] (Fig. 4a, Extended Data Fig. 6a) and measured the rate of apically directed cell extrusions via time-lapse microscopy. HU treatment increased the rate of cell extrusion from the MDCK-II monolayer by more than threefold over vehicle control (Fig. 4b, c, Supplementary Videos 6, 7). Using MDCK-Fucci cells, which produce a cell-cycle phase-specific fluorescence (G0/G1, red; S/G2/M, green), we found that cells extruded stochastically from the monolayers (as observed with vehicle treatment) mostly exhibited red fluorescence indicative of the G0 or G1 phase (Fig. 4d). By contrast, most cells extruded from HU-treated monolayers displayed green fluorescence, consistent with S-phase arrest (Fig. 4d).

Several observations indicate that cell death (for example, apoptosis) did not cause the HU-mediated cell extrusions: (i) similar percentages of HU-induced and stochastically extruded cells showed trypan blue staining (Fig. 4e); (ii) cells extruded following HU treatment were viable and proliferated within 24 h of being cultured in fresh medium (Fig. 4f); and (iii) the caspase inhibitor zVAD-FMK did not prevent HU-induced cell extrusion (Fig. 4g, Extended Data Fig. 6b). These findings demonstrate that HU induces the extrusion of living cells.

Last, we tested the requirement for ATR and CHK1 in replication stress-mediated extrusions from MDCK-II cell layers. HU treatment significantly increased the level of phosphorylated ATR (pATR) in MDCK-II cells (Fig. 4h, Extended Data Fig. 6c). Also, the small molecule CHK1 inhibitors SB 218078 and PF477736 suppressed HU-induced cell extrusion (Fig. 4g, Extended Data Fig. 6b), indicating that HU-induced mammalian cell extrusion requires the ATR–CHK1 pathway. In mammals, the ATR–CHK1-mediated replication-stress response activates p53[23]. HU treatment increased p53 levels, as did treatment with Nutlin-3, a chemical activator of p53 (Extended Data Fig. 6d, e). Furthermore, the p53 inhibitor pifithrin-α (PFT) completely suppressed HU-induced cell extrusion (Fig. 4g, Extended Data Fig. 6b). Although Nutlin-3 increased extrusion rates of MDCK-II cells (Fig. 4g), it did not result in replication stress (Fig. 4a, Extended Data Fig. 6a), indicating that p53 activation is sufficient to induce cell extrusion in the absence of replication stress.

## Discussion

Our findings are summarized in Fig. 4i and suggest the following four-step mechanistic model for replication-stress induced cell extrusion (Fig. 4j): (i) a cell in S phase experiences replication stress following a genotoxic insult (for example, HU) or the inheritance of insufficient replicative resources from an unequal cell division; (ii) ATR and CHK1 (and p53 in mammals) mediate a replication-stress response; (iii) cell adhesion molecules are downregulated[3], possibly through inhibition of CDK1, a regulator of cell adhesion during S phase[24]; and (iv) the cell is extruded as a consequence of this reduced adhesion[25] and mechanical forces generated by neighbouring cells (for example, constrictive forces preceding ventral enclosure in developing *C. elegans* embryos[26]) or physiological crowding[27].

Our finding that replication stress drives cell elimination by extrusion for both *C. elegans* and mammalian cells demonstrates that cell extrusion in *ced-3(lf)* embryos is not simply a result of the genetic perturbation of the caspase-mediated apoptosis pathway and indicates that this mechanism is evolutionarily conserved. The cell cycle is similarly conserved and is ancient. As cell elimination caused by an inducible cell-cycle state does not require specialized molecular or cellular machinery (unlike caspase-mediated apoptosis and phagocytosis), we propose that replication-stress-driven cell extrusion is a primordial process of cell elimination. The observation that cells targeted for caspase-dependent cell death extrude when caspases are inactivated suggests that extrusion as a primitive form of cell elimination has in some instances been supplanted by caspase-mediated apoptosis. We further suggest that a developmentally controlled replication-stress response might be used by metazoans for cell elimination via extrusion in a variety of biological contexts.

Replication stress and cell extrusion are key features of cancer biology[1,28], but their relationship has not been explored. We propose that the extrusion of cells undergoing replication stress can be tumour-suppressive. Non-cancerous cells that fail to respond to replication stressors can accrue DNA damage, genomic rearrangements and ploidy defects associated with oncogenesis[28]. Pre-cancerous and cancerous cells experience persistent replication stress[28] resulting from the overexpression, amplification or mutational activation of genes that drive uncontrolled proliferation. In such contexts, cell extrusion activated by replication stress could function as an early checkpoint to eliminate pre-cancerous and malignant cells.

In other contexts, cell extrusion induced by replication stress might be subverted to promote metastatic tumorigenesis. Indeed, the mouse p53 R172H mutation (equivalent to the R175H mutation common to human tumours) causes a high frequency of metastatic tumours[29,30]. Mouse p53(R172H) induces a replication-stress response by increasing both CHK1 expression and basal CHK1 phosphorylation[31,32]. We suggest that this ectopic replication-stress response triggers the extrusion of cells harbouring this mutation and that an oncogenic mutation in APC or K-RAS[5], or perhaps p53(R172H) itself, reverses the direction of extrusion from apical (causing elimination) to basal (causing dissemination) to promote metastasis. In addition, reports that chemotherapeutic inhibitors of DNA replication, such as doxorubicin and cyclophosphamide, promote the metastatic spread of tumour cells[33] also support this notion.

In short, we have identified a conserved mechanism that links replication stress to the process of cell extrusion. We suggest that cell extrusion driven by replication stress is a primordial mechanism of cell elimination common to all metazoa and that cell extrusion arising from replication stress regulates the survival and spread of tumour cells.

## Online content

Any methods, additional references, Nature Research reporting summaries, source data, extended data, supplementary information, acknowledgements, peer review information; details of author contributions and competing interests; and statements of data and code availability are available at https://doi.org/10.1038/s41586-021-03526-y.


1. Ohsawa, S., Vaughen, J. & Igaki, T. Cell extrusion: a stress-responsive force for good or evil in epithelial homeostasis. *Dev. Cell* **44**, 284–296 (2018).
2. De Goeij, J. M. et al. Cell kinetics of the marine sponge *Halisarca caerulea* reveal rapid cell turnover and shedding. *J. Exp. Biol.* **212**, 3892–3900 (2009).
3. Denning, D. P., Hatch, V. & Horvitz, H. R. Programmed elimination of cells by caspase-independent cell extrusion in *C. elegans*. *Nature* **488**, 226–230 (2012).
4. Rosenblatt, J., Raff, M. C. & Cramer, L. P. An epithelial cell destined for apoptosis signals its neighbors to extrude it by an actin- and myosin-dependent mechanism. *Curr. Biol.* **11**, 1847–1857 (2001).
5. Gudipaty, S. A. & Rosenblatt, J. Epithelial cell extrusion: pathways and pathologies. *Semin. Cell Dev. Biol.* **67**, 132–140 (2017).
6. Timson, J. Hydroxyurea. *Mutat. Res.* **32**, 115–132 (1975).
7. Koç, A., Wheeler, L. J., Mathews, C. K. & Merrill, G. F. Hydroxyurea arrests DNA replication by a mechanism that preserves basal dNTP pools. *J. Biol. Chem.* **279**, 223–230 (2004).
8. Takeda, D. Y. & Dutta, A. DNA replication and progression through S phase. *Oncogene* **24**, 2827–2843 (2005).
9. Fay, D. S. & Han, M. Mutations in *cye-1*, a *Caenorhabditis elegans* cyclin E homolog, reveal coordination between cell-cycle control and vulval development. *Development* **127**, 4049–4060 (2000).
10. van Rijnberk, L. M., van der Horst, S. E. M., van den Heuvel, S. & Ruijtenberg, S. A dual transcriptional reporter and CDK-activity sensor marks cell cycle entry and progression in *C. elegans*. *PLoS One* **12**, e0171600 (2017).
11. Brauchle, M., Baumer, K. & Gönczy, P. Differential activation of the DNA replication checkpoint contributes to asynchrony of cell division in *C. elegans* embryos. *Curr. Biol.* **13**, 819–827 (2003).
12. Zerjatke, T. et al. Quantitative cell cycle analysis based on an endogenous all-in-one reporter for cell tracking and classification. *Cell Rep.* **19**, 1953–1966 (2017).

13. Teuliere, J. & Garriga, G. Size matters: how *C. elegans* asymmetric divisions regulate apoptosis. *Results Probl. Cell Differ.* **61**, 141–163 (2017).
14. Stergiou, L., Eberhard, R., Doukoumetzidis, K. & Hengartner, M. O. NER and HR pathways act sequentially to promote UV-C-induced germ cell apoptosis in *Caenorhabditis elegans*. *Cell Death Differ.* **18**, 897–906 (2011).
15. Dinant, C. et al. Activation of multiple DNA repair pathways by sub-nuclear damage induction methods. *J. Cell Sci.* **120**, 2731–2740 (2007).
16. Wu, Y. C., Stanfield, G. M. & Horvitz, H. R. NUC-1, a *Caenorhabditis elegans* DNase II homolog, functions in an intermediate step of DNA degradation during apoptosis. *Genes Dev.* **14**, 536–548 (2000).
17. Toledo, L. I. et al. ATR prohibits replication catastrophe by preventing global exhaustion of RPA. *Cell* **155**, 1088–1103 (2013).
18. Stevens, H., Williams, A. B. & Michael, W. M. Cell-type specific responses to DNA replication stress in early *C. elegans* embryos. *PLoS One* **11**, e0164601 (2016).
19. Ossareh-Nazari, B., Katsiarimpa, A., Merlet, J. & Pintard, L. RNAi-based suppressor screens reveal genetic interactions between the CRL2LRR-1 E3-ligase and the DNA replication machinery in *Caenorhabditis elegans*. *G3 (Bethesda)* **6**, 3431–3442 (2016).
20. Sonneville, R. et al. CUL-2$^{LRR-1}$ and UBXN-3 drive replisome disassembly during DNA replication termination and mitosis. *Nat. Cell Biol.* **19**, 468–479 (2017).
21. Dewar, J. M., Low, E., Mann, M., Räschle, M. & Walter, J. C. CRL2$^{Lrr1}$ promotes unloading of the vertebrate replisome from chromatin during replication termination. *Genes Dev.* **31**, 275–290 (2017).
22. Merlet, J. et al. The CRL2LRR-1 ubiquitin ligase regulates cell cycle progression during *C. elegans* development. *Development* **137**, 3857–3866 (2010).
23. Meek, D. W. Tumour suppression by p53: a role for the DNA damage response? *Nat. Rev. Cancer* **9**, 714–723 (2009).
24. Jones, M. C., Askari, J. A., Humphries, J. D. & Humphries, M. J. Cell adhesion is regulated by CDK1 during the cell cycle. *J. Cell Biol.* **217**, 3203–3218 (2018).
25. Grieve, A. G. & Rabouille, C. Extracellular cleavage of E-cadherin promotes epithelial cell extrusion. *J. Cell Sci.* **127**, 3331–3346 (2014).
26. Wernike, D., Chen, Y., Mastronardi, K., Makil, N. & Piekny, A. Mechanical forces drive neuroblast morphogenesis and are required for epidermal closure. *Dev. Biol.* **412**, 261–277 (2016).
27. Eisenhoffer, G. T. et al. Crowding induces live cell extrusion to maintain homeostatic cell numbers in epithelia. *Nature* **484**, 546–549 (2012).
28. Gaillard, H., García-Muse, T. & Aguilera, A. Replication stress and cancer. *Nat. Rev. Cancer* **15**, 276–289 (2015).
29. Olive, K. P. et al. Mutant p53 gain of function in two mouse models of Li-Fraumeni syndrome. *Cell* **119**, 847–860 (2004).
30. Lang, G. A. et al. Gain of function of a p53 hot spot mutation in a mouse model of Li-Fraumeni syndrome. *Cell* **119**, 861–872 (2004).
31. Singh, S. et al. Mutant p53 establishes targetable tumor dependency by promoting unscheduled replication. *J. Clin. Invest.* **127**, 1839–1855 (2017).
32. Yeo, C. Q. X. et al. p53 maintains genomic stability by preventing interference between transcription and replication. *Cell Rep.* **15**, 132–146 (2016).
33. Karagiannis, G. S. et al. Neoadjuvant chemotherapy induces breast cancer metastasis through a TMEM-mediated mechanism. *Sci. Transl. Med.* **9**, eaan0026 (2017).

# Methods

## Strains

*C. elegans* hermaphrodite strains were maintained on nematode growth medium (NGM) plates containing 3 g/l NaCl, 2.5 g/l peptone and 17 g/l agar supplemented with 1 mM $CaCl_2$, 1 mM $MgSO_4$, 1 mM $KPO_4$ and 5 mg/l cholesterol with *E. coli* OP50 as a source of food[34]. All strains were derived from Bristol N2. *ced-3(lf)* refers to the *n3692* deletion allele of *ced-3*[3]. *cye-1(lf)* refers to the *eh10* allele of *cye-1*[35]. *ced-5(lf)* refers to the *n1812* allele of *ced-5*[36]. *C. elegans* strains carrying the transgenes *nIs861* and *isIs17* were maintained at 25 °C. All other strains were maintained at 22 °C. The transgenes and mutations used are listed below:

LGI: *nIs433[$P_{pgp\text{-}12}$::4xNLS::GFP::unc-54 3′UTR; p76-16B(unc-76(+))]*, *cye-1(eh10)*

LGII: *heSi192[$P_{eft\text{-}3}$::tDHB::eGFP::tbb-2 3′UTR + Cbr-unc119(+)]*

LGIII: *unc-119(ed3)*

LGIV: *ced-3(n3692)*, *ced-5(n1812)*

LGV: *ltIs44[$P_{pie\text{-}1}$::mCherry::PH(PLC1delta1) + unc-119(+)]*

LGX: *nIs434[$P_{pgp\text{-}12}$::4xNLS::GFP::unc-54 3′UTR; p76-16B(unc-76(+))]*

Unknown linkage: *stIs10026[$P_{his\text{-}72}$::HIS-72::GFP]*, *isIs17[pGZ295($P_{pie\text{-}1}$::GFP ::pcn-1(W03D2.4))*, *pDP#MM051 (unc-119(+))]*, *nIs861[pDD111($P_{egl\text{-}1}$::mCherry::PH::unc-54 3′UTR)]*, *nIs632[pDD111($P_{egl\text{-}1}$::mCherry::PH::unc-54 3′UTR)*, *pML902 (dlg-1::GFP)*, *p76-16B(unc-76(+))]*, *opIs263[$P_{rpa\text{-}1}$::rpa-1::YFP + unc-119(+)]*

Extrachromosomal array: *nEx3043[cye-1(+); $P_{sur\text{-}5}$::RFP]*

*nIs632* and *nIs861* express membrane-localized mCherry from the *egl-1* promoter, which facilitated the identification of ABplpappap (an *egl-1*-expressing cell). *nIs632* does not express *dlg-1::GFP*, presumably as a result of partial transgene silencing[37–39]. *stIs10026*[40] ubiquitously expresses a GFP-tagged histone HIS-72 from its endogenous promoter, which produces fluorescence in the nuclei of all cells and helps to highlight extruded cells with respect to surrounding unextruded cells.

The following strains were used: N2 (Wild-type strain), MT4434 *ced-5(n1812) IV*, MT12054 *ced-3(n3692) IV*, MT20083 *nIs433 I*, MT20084 *nIs434 X*, MT20117 *nIs433 I; ced-3(n3692) IV*, MT20131 *ced-3(n3692) IV; nIs434 X*, MT26340 *cye-1(eh10)/hT2[qIs48] I; hT2[qIs48]/+ III; nIs434 X*, MT26342 *cye-1(eh10)/hT2[qIs48] I; hT2[qIs48]/+ III; ced-3(n3692) IV; nIs434 X*, MT26360 *cye-1(eh10)/hT2[qIs48] I; hT2[qIs48]/+ III; ced-3(n3692) IV; nIs434 X; nEx3043*, MT22450 *ced-3(n3692) IV; stIs10026; nIs632*, MT25639 *ced-3(n3692) IV; stIs10026; nIs861*, MT25640 *heSi192 II; ced-3(n3692) IV; nIs861*, MT25692 *ced-3(n3692) IV; ltIs44 V; stIs10026*, MT25807 *ced-3(n3692) IV; nIs861; isIs17*, MT26335 *ced-3(n3692) IV; ltIs44 V; opIs263*.

Strains MT25640, MT25692, MT25807 and MT26335 might carry the *unc-119(ed3)* mutation in the background, which is rescued by the transgenes *heSi192*, *ltIs44*, *isIs17* and *ltIs44* in these strains, respectively.

## Plasmids and fosmids

pDD111 (*$P_{egl\text{-}1}$::mCherry::PH::unc-54 3′UTR*) was generated with the following steps: i) 6.8 kb of the *egl-1* promoter was amplified from genomic DNA with Phusion DNA polymerase using the primers 5′-CGCCTGCAGTTGAAATTTGGGGATATTTTGG-3′ and 5′- CGC GAGCTCCTGGAAATTAGTAAGGTTTTGAAGGGGG-3′; ii) the amplicon was digested with PstI and SacI (New England Biolabs) and ligated into pPD122.56, which encodes 4×NLS–GFP to generate *$P_{egl\text{-}1}$::4xNLS::GFP::unc-54 3′UTR*; iii) mCherry–PH (pleckstrin homology) sequence was amplified from pAA173 using primers 5′-CGCACCGGTCCAGATGGCTCAAACAAAGC-3′ and 5′- CGCGAATTC GGCACAAGTTCATTCACAGG-3′ and digested with EcoRI and AgeI (New England Biolabs) and ligated into pDD122.56 (*$P_{egl\text{-}1}$::4xNLS::GFP ::unc-54 3′UTR*), which generated the plasmid pDD122.56 (*$P_{egl\text{-}1}$::4xNL S::mCherry::PH::unc-54 3′UTR*); iv) the 4×NLS sequence was removed with the primers 5′- ggagctcAGAAAAAATGGTCTCAAAGGGTG-3′ and 5′- CACCCTTTGAGACCATTTTTTCTGAGCTCC-3′ using QuikChange Site-Directed Mutagenesis (Agilent) to generate pDD111 (*$P_{egl\text{-}1}$::mCher rry::PH::unc-54 3′UTR*).

Sequences of all RNAi constructs that affected cell extrusion are provided in the Supplementary Information. RNAi clones were constructed for *atl-1*, *mat-2* and *lin-15B*. Genomic regions of about 1 kb length were amplified from wild-type genomic lysates using Q5 Hot Start high-fidelity polymerase (New England Biolabs) with the following primers:

*atl-1*: 5′-TCGAATTCCTGCAGCTCCTCGAACCCATCATCCCT-3′; 5′-TGACGCGTGGATCCCATGAAGCTGCGTGGTTGTTG-3′. *mat-2*: 5′-TCGAATTCCTGCAGCCTGGAACTCATCCCATACGC-3′; 5′-TGACGCGT GGATCCCCATTGGAACCTCCAGATGCT-3′. *lin-15B*: 5′-TCGAAT TCCTGCAGCGCTGACACAATTGCGAACAT-3′; 5′-TGACGCGTGGATCCC CGTGTGCATAAAGACCAAGG-3′. *atl-1* + *chk-1*: *atl-1* fragment 5′-TCGAATTCCTGCAGCTCCTCGAACCCATCATCCCT-3′; 5′- ACACGACA GCGTCCGCAGAAATGAAGCTGCGTGGTTGTTG-3′; *chk-1* fragment 5′-TTCTGCGGACGCTGTCGTGTCAAGCGGATCCGTGGTATCA-3′; 5′- TGA CGCGTGGATCCCCCGAGTGCTCCACATTGACT-3′.

These inserts were cloned into the pL4440 vector linearized with XmaI (New England Biolabs) using the In-Fusion HD cloning kit (TaKaRa) according to the manufacturer's instructions. The cloned vector was then transformed into competent HT115 bacterial cells. Correct RNAi clones were identified by Sanger sequencing. Geneious 10.2.6 (Biomatters, Inc.) was used to guide all plasmid design and construction.

The fosmid WRM0637bF05 (Source Bioscience), which contains the genomic *cye-1* sequence, was used for genomic rescue of the Tex phenotype in *cye-1(eh10); ced-3(n3692); nIs434* animals. A plasmid containing the sequence for *$P_{sur\text{-}5}$::RFP*, which expresses RFP cell-autonomously, was used as a fluorescent marker of cells carrying a mitotically unstable extrachromosomal array for genetic mosaic analysis.

## Germline transformation

Germline transformation experiments were performed as described[41]. To generate the *cye-1*-rescuing transgene *nEx3043*, the fosmid WRM0637bF05, a plasmid containing the sequence for *$P_{sur\text{-}5}$::RFP* and 1 kb plus DNA ladder (Invitrogen), was injected into *hT2[qIs48]/ cye-1(eh10); ced-3(n3692); nIs434* animals at 3 ng/µl, 20 ng/µl and 80 ng/µl.

## RNAi treatments

Previously described feeding RNAi constructs and reagents were used to perform RNAi feeding experiments[42,43]. In brief, HT115 *E. coli* bacteria carrying RNAi clones in the pL4440 vector were grown for at least 12 h in Luria broth (LB) liquid medium with 75 mg/l ampicillin at 37 °C. These cultures were seeded onto 6-cm Petri plates with NGM containing 1 mM isopropyl-β-D-thiogalactopyranoside (IPTG) (Amresco) and 75 mg/l ampicillin and incubated for 24 h at 22 °C. For imaging experiments using confocal microscopy, ten L4 animals were added to each RNAi plate and imaging of progeny embryos was performed on the next day as described in 'Microscopy' (below). For excretory cell counts, five L4 animals were added to each RNAi plate and L3–L4 progeny were scored for the number of excretory cells, as described in 'Excretory cell counts' (below). If a bacterial clone targeting a certain gene was not available in previously constructed libraries[42,44], we generated our own RNAi clone as described in 'Plasmids and fosmids' (above). Each RNAi experiment included an empty pL4440 vector negative control. Larvae and embryos were randomly selected for experiments after RNAi treatment. Experiments requiring imaging of *C. elegans* embryos after candidate RNAi treatments could not be effectively blinded, as the RNAi treatments produced developmental phenotypes that made the identity of the target gene obvious.

## Genome-wide RNAi screen

The ORFeome RNAi library was used to conduct a genome-wide RNAi screen[42]. For each day of the RNAi screen, all bacterial colonies from two 96-well plates were cultured for at least 12 h at 37 °C in LB with 75 mg/l ampicillin. These cultures were then pre-incubated with 1 mM

IPTG (Amresco) for 1 h to maximize induction of dsRNA production. We prepared 24-well plates with each well containing 2 ml NGM with 1 mM IPTG (Amresco) and 75 mg/l ampicillin in advance and stored them at 4 °C until needed; they were brought to room temperature a few hours before seeding. Each bacterial colony culture was then seeded onto an individual well of a 24-well plate and incubated for 24 h at 20 °C. Three L4 animals were picked into a 10-µl drop of M9 medium, which facilitated their transfer into a well using a pipette. The progeny of these three animals were screened 3 days later. Each set of RNAi clones screened also included a *pig-1* RNAi positive control and an empty pL4440 vector negative control. The scorer was blinded to the identity of the RNAi clones. Excretory cell counts were performed as described in 'Excretory cell counts' (below). Sanger sequencing was used to confirm the identities of RNAi clones that reproducibly generated a Tex phenotype for more than 10% of the animals scored.

### Microscopy

All RNAi screens scoring excretory cells were performed using a Nikon SMZ18 fluorescent dissecting microscope.

DIC and epifluorescence images of L3-L4 larval stage animals carrying the transgene *nIs433[$P_{pgp\text{-}12}$::4xNLS-GFP]* or *nIs434[$P_{pgp\text{-}12}$::4xNLS-GFP]*, which mark the excretory cell and ectopic excretory-like cells, were obtained using a 63× objective lens (Zeiss) on an AxioImager Z2 (Zeiss) compound microscope and Zen Blue software (Zeiss).

For confocal microscopy of cell extrusion (or its absence) from *ced-3(lf)* embryos, embryos staged at the 200–300-cell stage were picked and mounted onto a glass slide (Corning) with a freshly prepared 2% agarose pad. Embryos with ventral surfaces facing the objective were selected for imaging. Confocal images of embryos were obtained using a 63× objective lens (Zeiss) on a Zeiss LSM800 confocal microscope.

For observing extrusion (or absence of extrusion) from *ced-3(lf)* embryos, we focused particularly on the cell ABplpappap, the identification of which is facilitated by its central position on the ventral surface[45]. The fluorescent transgene *nIs861[$P_{egl\text{-}1}$::mCherry::PH]* or *nIs632[$P_{egl\text{-}1}$::mCherry::PH; dlg-1::GFP]*, which express the Pleckstrin homology domain of PLC-δ fused to mCherry from the promoter of *egl-1*, was used to label the membrane of the ABplpappap cell, an *egl-1*-expressing cell[3], to further facilitate cell identification. Another fluorescent transgene (*stIs10026[his-72::GFP]*, which expresses GFP-tagged HIS-72 histone protein) was used to label the nuclei of all cells to help to define ABplpappap's location within the embryo. Time-lapse confocal microscopy was used to monitor the location of ABplpappap in embryos, keeping the cell in view by refocusing on it every 30 s. Confocal imaging during a period of about 50 min ending in ventral enclosure (the point at which hypodermal cells meet on the ventral surface of the embryo) was sufficient to determine whether ABplpappap did or did not undergo extrusion. To determine whether specific RNAi treatments caused cell extrusion from wild-type embryos, RNAi-treated embryos were examined using a 63× objective lens (Zeiss) on a Zeiss LSM800 confocal compound microscope for the presence of one or more cell(s) outside the embryonic body and some such embryos with extruded cells were imaged.

To determine whether ABplpappap and other cells that are extruded entered the cell cycle, embryos carrying the transgene *heSi192[$P_{eft\text{-}3}$::tDHB::eGFP::tbb-2 3′UTR]* expressing a codon-optimized (for *C. elegans*) C-terminal fragment of human DNA helicase B, which translocates from the nucleus to the cytoplasm in response to the activity of the cell cycle CDKs 1 and 2[10], were examined using confocal microscopy after various RNAi treatments. *nIs861* labelled the membrane of ABplpappap with mCherry and facilitated cell identification in these embryos.

To determine the cell cycle phase of ABplpappap and other cells that are extruded, embryos carrying the transgene *isIs17[$P_{pie\text{-}1}$::GFP::PCN-1]* expressing GFP-tagged PCN-1 protein, which produces a phase-specific fluorescence intensity and localization pattern[11], were examined using confocal microscopy after various RNAi treatments. *nIs861* labelled the membrane of ABplpappap with mCherry and facilitated cell identification in these embryos.

For examining ABplpappap and other extruded cells for replication stress, embryos carrying the transgene *opIs263[$P_{rpa\text{-}1}$::rpa-1::YFP]* expressing YFP-tagged RPA-1, which localizes to foci under conditions of replication stress[14], were examined using confocal microscopy after various RNAi treatments. *ltIs44[$P_{pie\text{-}1}$::mCherry::PH]* labelled the membrane of all cells with mCherry and facilitated the identification of cell boundaries in these embryos.

Microscopy for the genetic mosaic analysis experiments are described in the 'Mosaic analysis' section below.

Images were processed with ImageJ software (NIH), Photoshop CC 2019 (Adobe) and Illustrator CC 2019 (Adobe) software. The Time Stamper function in the Stowers ImageJ plugin was used to mark elapsed time on time-lapse videos.

### Excretory cell counts

Excretory cell counts were performed using a dissecting microscope equipped with fluorescence at a total magnification of 270×. For the genome-scale RNAi screen, roughly 50 animals were examined in each well of a 24-well plate, and any well with more than five animals with two excretory cells was marked for confirmatory testing. Excretory cell counts in confirmatory RNAi experiments, candidate RNAi experiments and experiments with genetic mutants were conducted using 6-cm Petri plates with appropriate medium. Animals were first immobilized by keeping the Petri plates on ice for 30 min. At least 100 animals at the L3–L4 larval stage were scored for each genotype or RNAi experiment unless there was extensive lethality or a growth defect, in which case a lower number or earlier-stage animals, respectively, were scored. A cell was scored as an excretory or an excretory-like cell if it were located in the anterior half of the animal and its nucleus had strong GFP expression.

### Mosaic analysis

To perform mosaic analysis, transgenic animals of the genotype *hT2[qIs48]/cye-1(eh10); ced-3(n3692); nIs434; nEx3043[cye-1(+); $P_{sur\text{-}5}$::RFP]* were generated. Progeny of animals that lost the *hT2* balancer and were of the genotype *cye-1(eh10); ced-3(n3692); nIs434; nEx3043* were examined for the Tex phenotype. Ten such animals that displayed the Tex phenotype despite carrying the *cye-1*-rescuing array were examined using confocal microscopy with 63× (Zeiss) or 100× (Zeiss) objective lenses for the presence of the RFP-expressing extrachromosomal array in multiple cells, including the excretory cell (identified by the presence of distinctive canals extending from the cell body) and ABplpappap. Because the majority of these animals showed the presence of the rescuing array in the excretory cell, but not in ABplpappap, only the sublineage containing these cells was further analysed.

### Calculation of cell size

Confocal micrographs were obtained for multiple focal planes starting at the ventral surface and ending at the dorsal surface of the embryo, with each plane separated by a distance of 0.37 µm. The greatest area occupied by a cell in any plane was designated the 'maximum area' of a cell.

To determine the ratio of diameters of ABplpappaa and ABplpappap, the square root of the mean of the area ratios was calculated and the two cells were assumed to be perfect spheres.

### Generation of virtual lateral sections

Confocal micrographs were obtained for multiple focal planes starting at the ventral surface and ending at the dorsal surface of embryos that had completed epidermal ventral enclosure, with each plane separated by a distance of 0.37 µm.

A virtual lateral section for each *Z*-stack was generated at the plane perpendicular to the left–right axis that bisected ABplpappap using the Orthogonal Views function of Fiji[46].

### Fluorescence signal quantification

**tDHB–GFP.** The ABplpappap nuclear boundary, cell membrane boundary and tDHB–GFP fluorescence signal were identified using the DIC, mCherry and GFP channels, respectively, of confocal images of RNAi-treated *ced-3(lf)* embryos expressing the transgenes *heSi192* and *nIs861*. Mean tDHB–GFP fluorescence intensities inside the nuclear region, entire cell and background were quantified using Fiji software[46]. Mean cytoplasmic tDHB–GFP fluorescence intensity was calculated using the formula $I_{cytoplasm} = ((I_{cell} \times \text{cell area}) - (I_{nucleus} \times \text{nucleus area}))/(\text{cell area} - \text{nucleus area})$, where $I_{cytoplasm}$, $I_{cell}$ and $I_{nucleus}$ denote the mean tDHB fluorescence intensity in the cytoplasm, cell and nucleus, respectively. The ratio of nuclear-to-cytoplasmic tDHB fluorescence intensity in Fig. 2c was adjusted for background fluorescence (measured from a random area outside the embryo boundaries); that is, the background fluorescence intensity was subtracted from both nuclear and cytoplasmic fluorescence intensity values before the ratios were calculated.

**GFP–PCN-1 and RPA-1–YFP.** The ABplpappap nucleus was identified from the DIC channel of confocal images of RNAi-treated *ced-3(lf)* embryos expressing the corresponding transgenes. The coefficient of variation (ratio of s.d. to mean) of fluorescence intensity inside the nuclear region was used as a measure to differentiate between diffuse and punctate fluorescence signals and was quantified using Fiji software[46]. In brief, highly localized fluorescence signals were expected to have pixel fluorescence intensity values that were either much higher or much lower than the mean fluorescence intensity of an area of interest, whereas a diffuse fluorescence signal was expected to have pixel intensity values that were closer to the mean fluorescence intensity of an area of interest. A high variation from the mean would produce a high variance and hence a higher standard deviation and vice versa. As standard deviation is also influenced by fluorescence intensity, we used coefficient of variation as a measure of signal localization to remove any artefactual differences in fluorescence intensity among embryos.

### TUNEL staining

TUNEL staining was performed as described[16] with the following modifications. After being frozen with liquid nitrogen, the embryos were fixed with 4% PFA/PBS, pH 7.4 for 15 min at room temperature and then permeabilized by incubation with 0.1% Triton X-100 in PBS for 10 min at room temperature. After washing, TUNEL staining was performed according to the manufacturer's (Roche, Switzerland) instructions. Stained embryos were mounted using Fluoroshield with DAPI mounting solution (Sigma-Aldrich) to visualize the nuclei.

### Cell culture

The MDCK-II[47] cells were obtained from European Collection of Authenticated Cell Cultures (ECACC, 00062107, 19G037). MDCK-Fucci[48] cells (originally generated in L. Hufnagel's laboratory) were a gift from X. Trepat. The MDCK-II cell line was authenticated before shipping by ECACC. The MDCK-Fucci cell line was not authenticated. Both cell lines were tested for mycoplasma contamination before shipping. Both cell lines were cultured in Dulbecco's modified Eagle's medium (DMEM) supplemented with 10% fetal bovine serum and 1% penicillin/streptomycin in a humidified incubator at 37 °C with 5% $CO_2$.

### Chemicals

We prepared 2 mM HU (Millipore Sigma, H8627) in culture medium before each experiment. Nutlin-3 (Tocris, 3984), Pifithrin-α (Focus Biomolecules, 10-2480), SB 218078 (Tocris, 2560), PF477736 (Tocris, 4277) and zVAD-FMK (Promega, G7231) stocks were prepared in DMSO and kept at −20 °C until needed, when dilutions were prepared in culture medium for cell treatment for final concentrations of 10 μM, 10 μM, 30 nM, 5 nM and 50 μM, respectively.

### Mammalian cell imaging

These assays were performed using 6-well plastic plates. Twenty thousand MDCK-II cells were seeded in each well and grown to confluence for 72 h. On the day of the experiment, cells were washed twice with PBS and treated with fresh medium or various chemicals in medium. After equilibration, plates were imaged at 15-min intervals for up to 24 h, using an Evos M7000 imaging system equipped with a humidified onstage incubator (37 °C, 5% $CO_2$). Several positions per well were imaged in the phase contrast and green and red fluorescence channels (when applicable) available in this system.

### Mammalian cell extrusion quantification

In time-lapse phase contrast images, extruding cells are easily identifiable as bright, white, rounded spots emerging from the epithelial plane. We counted the number of cells with these features for each condition using the Cell Counter plugin of Fiji[46]. The number of cell extrusions per XY position was quantified without knowing the corresponding treatment. Extrusions are reported as the number of extruding cells per hour for comparison between experiments of different duration.

### Mammalian cell-cycle phase determination

The Fucci system differentially labels the nuclei of cells in G1 (red) and S/G2/M (green) phases[49]. Images of MDCK-Fucci cells with HU or control treatment were obtained in the phase contrast, red and green fluorescence channels as described in 'Mammalian cell imaging' (above). For each position, a multi-channel stack was built using Fiji[46]. After we identified an extruded cell in the phase contrast channel, we determined the cell cycle phase using the fluorescence channels.

### Mammalian re-seeding experiments

At the end of an imaging experiment, supernatants were collected and centrifuged (1,200 rpm, 5 min, room temperature). Pellets were re-suspended in 50 μl PBS, and 10 μl of the suspension was used for cell counting with Trypan blue in a Neubauer chamber, allowing us to simultaneously calculate the number of cells being re-seeded and the fraction of cells that was dead. The remaining cells were seeded with 1 ml fresh medium in a 24-well plate and grown in the cell culture incubator. Images were obtained at 2 h and 24 h for cell counting.

### Mammalian cell immunostaining

Cells were fixed in 4% PFA-PBS for 20 min at 37 °C, permeabilized with 0.5% Triton X-100-PBS for 5 min at room temperature and stained with primary antibodies (all 1:250 in 1% BSA-PBS: p53, abcam ab26; phospho-ATR (Ser248), ThermoFisher 720107; phospho-histone H2A.X (Ser139), Cell Signaling 9718) overnight at 4 °C, and secondary antibodies (with 1:500 AF647 phalloidin and 30 μg/ml Hoechst) for 1 h at room temperature. We used 1× PBS for washing between steps and preparation of all solutions. Samples were mounted with Fluoromount-G Mounting Medium (Invitrogen 00-4958-02).

### Fixed mammalian cell imaging

Samples were imaged using 20× air and 60× oil objectives of a Nikon Eclipse Ti2-E microscope equipped with a Yokogawa CSU-W1 spinning disk system, an Andor DU-888 camera, and a Toptica multi-laser bed. All settings were kept constant between conditions.

### Quantification of mammalian cell staining

All images were quantified with ad hoc Cell Profiler[50] pipelines. In brief, the IdentifyPrimaryObjects, MeasureObjectIntensity, and ExportToSpreadsheet modules were used sequentially for nuclear segmentation (Hoechst channel), nuclear intensity measurements (p53, pATR, or γH2AX channels) and data export, respectively. Cell staining analysis was automated, reducing the risk of human-originated bias.

### Statistics and reproducibility

All experiments were repeated independently at least three times to ensure reproducibility. All representative micrographs are one example of five to ten biologically independent replicates of the same experiment, of which the remaining micrographs or quantification as a graph are provided in an associated figure panel, or have been described in the main text.

For calculation of statistical significance for fluorescence intensity and area ratios, the ratios were first transformed to logarithm values, with the assumption that logarithm of ratios produced a normal distribution of values. Normal distributions with unequal variances were assumed for coefficients of variance of GFP–PCN-1 and RPA-1–YFP signal fluorescence intensity. Normal distributions with unequal variances were assumed for rates of extrusion after different chemical treatments. No assumptions were made about the distributions of the rates of cell death under HU and vehicle treatments. Normal distributions with unequal variances were assumed for the fraction of extruded cells in different phases of the cell cycle after HU and vehicle treatments. Normal distribution was assumed for numbers of cells reseeded in fresh medium after pre-treatment in different conditions. As each mammalian-cell staining image contained from hundreds to thousands of cells, per-cell statistical analysis would result in extremely low *P* values. To avoid this sub-estimation, we first calculated descriptive statistics (median, average, s.d., *n*) for each image and made no assumptions about the distributions of these values for subsequent statistical analysis. All statistical analysis was performed using Prism (GraphPad Software). No statistical methods were used to predetermine sample size.

### Reporting summary

Further information on research design is available in the Nature Research Reporting Summary linked to this paper.

## Data availability

Data supporting all figures are available within the paper and in the associated Source Data files. Raw microscopy data are available upon request from the corresponding author. Source data are provided with this paper.


34. Brenner, S. The genetics of *Caenorhabditis elegans*. *Genetics* **77**, 71–94 (1974).
35. Brodigan, T. M., Liu, Ji., Park, M., Kipreos, E. T. & Krause, M. Cyclin E expression during development in *Caenorhabditis elegans*. *Dev. Biol*. **254**, 102–115 (2003).
36. Wu, Y. C. & Horvitz, H. R. *C. elegans* phagocytosis and cell-migration protein CED-5 is similar to human DOCK180. *Nature* **392**, 501–504 (1998).
37. Hsieh, J. et al. The RING finger/B-box factor TAM-1 and a retinoblastoma-like protein LIN-35 modulate context-dependent gene silencing in *Caenorhabditis elegans*. *Genes Dev*. **13**, 2958–2970 (1999).
38. Grishok, A., Sinskey, J. L. & Sharp, P. A. Transcriptional silencing of a transgene by RNAi in the soma of *C. elegans*. *Genes Dev*. **19**, 683–696 (2005).
39. Fischer, S. E. J. et al. Multiple small RNA pathways regulate the silencing of repeated and foreign genes in *C. elegans*. *Genes Dev*. **27**, 2678–2695 (2013).
40. Boeck, M. E. et al. Specific roles for the GATA transcription factors *end-1* and *end-3* during *C. elegans* E-lineage development. *Dev. Biol*. **358**, 345–355 (2011).
41. Mello, C. C., Kramer, J. M., Stinchcomb, D. & Ambros, V. Efficient gene transfer in *C.elegans*: extrachromosomal maintenance and integration of transforming sequences. *EMBO J*. **10**, 3959–3970 (1991).
42. Rual, J.-F. et al. Toward improving *Caenorhabditis elegans* phenome mapping with an ORFeome-based RNAi library. *Genome Res*. **14** (10B), 2162–2168 (2004).
43. Fraser, A. G. et al. Functional genomic analysis of *C. elegans* chromosome I by systematic RNA interference. *Nature* **408**, 325–330 (2000).
44. Kamath, R. S. et al. Systematic functional analysis of the *Caenorhabditis elegans* genome using RNAi. *Nature* **421**, 231–237 (2003).
45. Sulston, J. E., Schierenberg, E., White, J. G. & Thomson, J. N. The embryonic cell lineage of the nematode *Caenorhabditis elegans*. *Dev. Biol*. **100**, 64–119 (1983).
46. Schindelin, J. et al. Fiji: an open-source platform for biological-image analysis. *Nat. Methods* **9**, 676–682 (2012).
47. Hansson, G. C., Simons, K. & van Meer, G. Two strains of the Madin-Darby canine kidney (MDCK) cell line have distinct glycosphingolipid compositions. *EMBO J*. **5**, 483–489 (1986).
48. Streichan, S. J., Hoerner, C. R., Schneidt, T., Holzer, D. & Hufnagel, L. Spatial constraints control cell proliferation in tissues. *Proc. Natl Acad. Sci. USA* **111**, 5586–5591 (2014).
49. Sakaue-Sawano, A. et al. Visualizing spatiotemporal dynamics of multicellular cell-cycle progression. *Cell* **132**, 487–498 (2008).
50. McQuin, C. et al. CellProfiler 3.0: next-generation image processing for biology. *PLoS Biol*. **16**, e2005970 (2018).
51. Kipreos, E. T., Gohel, S. P. & Hedgecock, E. M. The *C. elegans* F-box/WD-repeat protein LIN-23 functions to limit cell division during development. *Development* **127**, 5071–5082 (2000).



**Acknowledgements** We thank S. van den Heuvel and the CGC, which is funded by NIH Office of Research Infrastructure Programs (P40 OD010440), for providing strains; L. Hufnagel and X. Trepat for providing MDCK-Fucci cells; G. van Meer and the ECACC for providing MDCK-II cells (ECACC 62107); N. An for strain management; S. Luo, S. R. Sando, E. L. Q. Lee, A. Doi, A. Corrionero and other members of the Horvitz laboratory for helpful discussions; and D. Ghosh, C. L. Pender, M. G. Vander Heiden, P. W. Reddien, and R. O. Hynes for suggestions regarding the manuscript. This work was supported by the Howard Hughes Medical Institute and by NIH grant R01GM024663. V.K.D. was a Howard Hughes Medical Institute International Student Research fellow. C.P.-P. was the recipient of Human Frontiers Science Program postdoctoral fellowship LT000654/2019-L. J.N.K. was supported by NIH grant R01GM024663. N.T. was supported by NIH Pre-Doctoral Training Grant T32GM007287. D.P.D. was supported by postdoctoral fellowships from the Damon Runyon Cancer Research Foundation and from the Charles A. King Trust. J.R. and C.P.-P. were funded by King's College London startup funds. H.R.H. is the David H. Koch Professor of Biology at MIT and an Investigator at the Howard Hughes Medical Institute.


**Author contributions** H.R.H. supervised the project. V.K.D. and H.R.H. conceptualized the project. V.K.D. and H.R.H. designed the experiments that used *C. elegans*. V.K.D., R.D., J.N.K. and N.T. performed the experiments that used *C. elegans*. V.K.D., R.D. and D.P.D. generated reagents. C.P.-P. and J.R. designed the experiments that used mammalian cells. C.P.-P. performed the experiments that used mammalian cells. V.K.D., D.P.D. and H.R.H. wrote the original and revised manuscript drafts. All authors contributed to data analysis, interpretation, and reviewing and editing of the manuscript.

**Competing interests** The authors declare no competing interests.

**Additional information**


**Supplementary information** The online version contains supplementary material available at https://doi.org/10.1038/s41586-021-03526-y.



**Correspondence and requests for materials** should be addressed to H.R.H.



**Peer review information** *Nature* thanks Joan Brugge and the other, anonymous, reviewer(s) for their contribution to the peer review of this work.

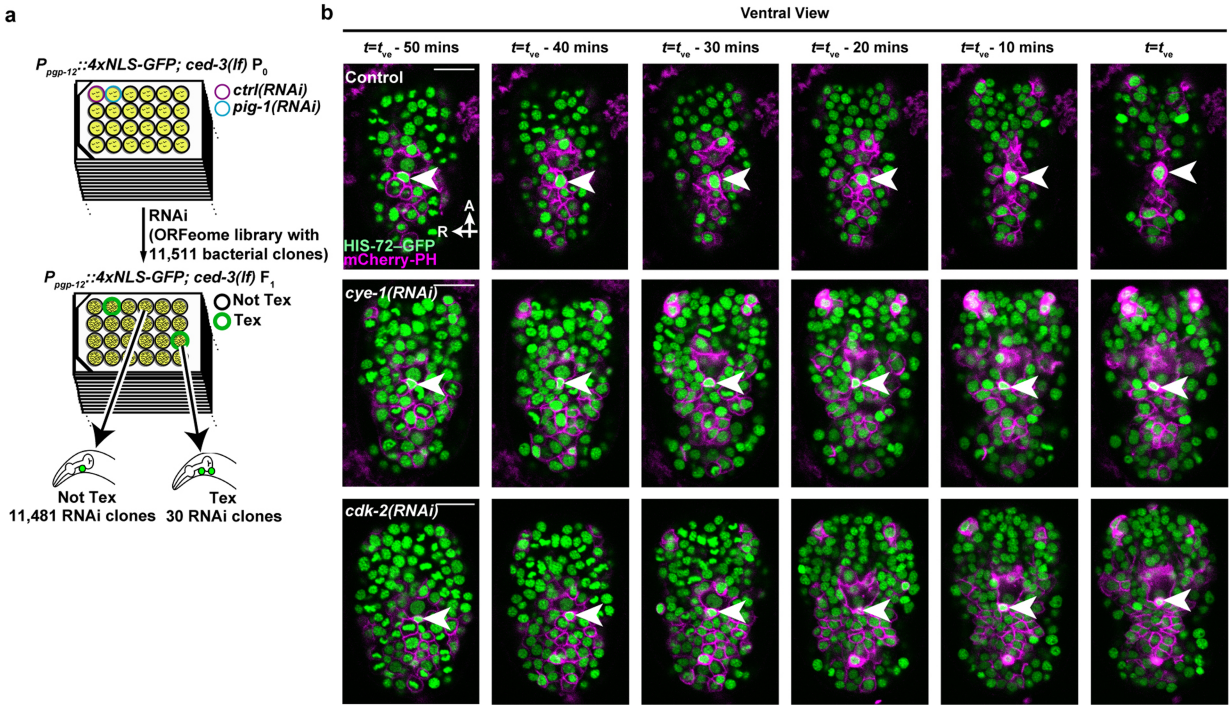


**Extended Data Fig. 1 | A genome-wide RNAi screen for the Tex phenotype revealed control of cell extrusion by *cye-1* and *cdk-2*.** **a**, Schematic representation of the genome-wide RNAi screen for the Tex phenotype. RNAi using pL4440 empty vector was used as negative control and *pig-1(RNAi)* was used as positive control[3]. **b**, Time-lapse confocal fluorescence micrographs of *ced-3(lf); stIs10026[his-72::GFP]; nIs632[$P_{egl-1}$::mCherry::PH]* embryos after indicated RNAi treatment at the indicated times. $t_{ve}$, time point of ventral enclosure. Arrowheads, ABplpappap. Scale bars, 10 µm.

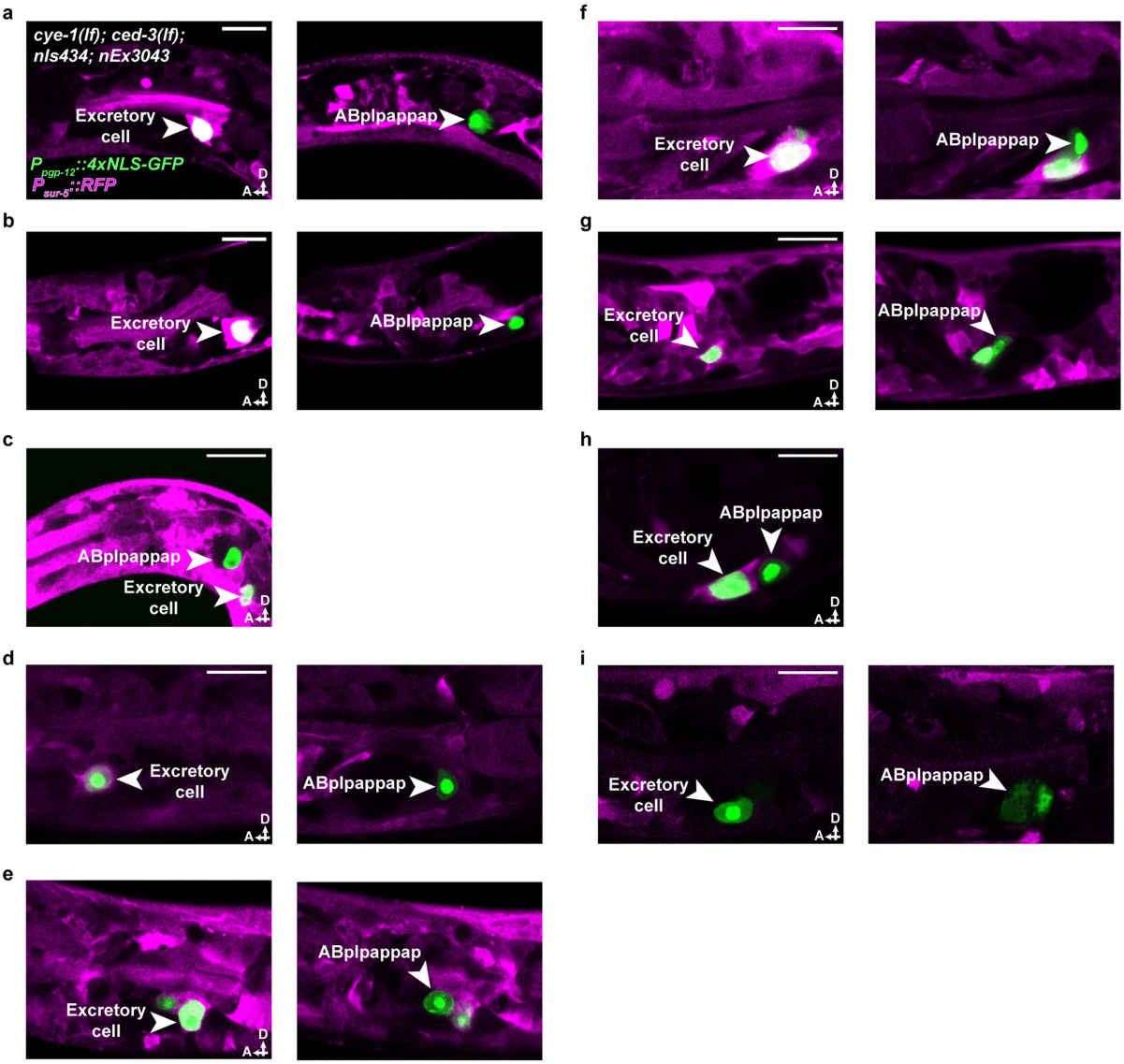


**Extended Data Fig. 2 | Genetically mosaic *cye-1(lf); ced-3(lf)* animals with the Tex phenotype lack a *cye-1*-rescuing transgene in ABplpappap.** **a**–**i**, Confocal micrographs showing the presence of the *cye-1(+)*-rescuing transgene in the excretory cell but not in ABplpappap (**a**–**h**) or in neither the excretory cell nor ABplpappap (**i**) of *cye-1(eh10); ced-3(n3692); nIs434[$P_{pgp-12}$::4xNLS-GFP]; nEx3043[cye-1(+); $P_{sur-5}$::RFP]* animals with the Tex phenotype. Scale bars, 10 µm.

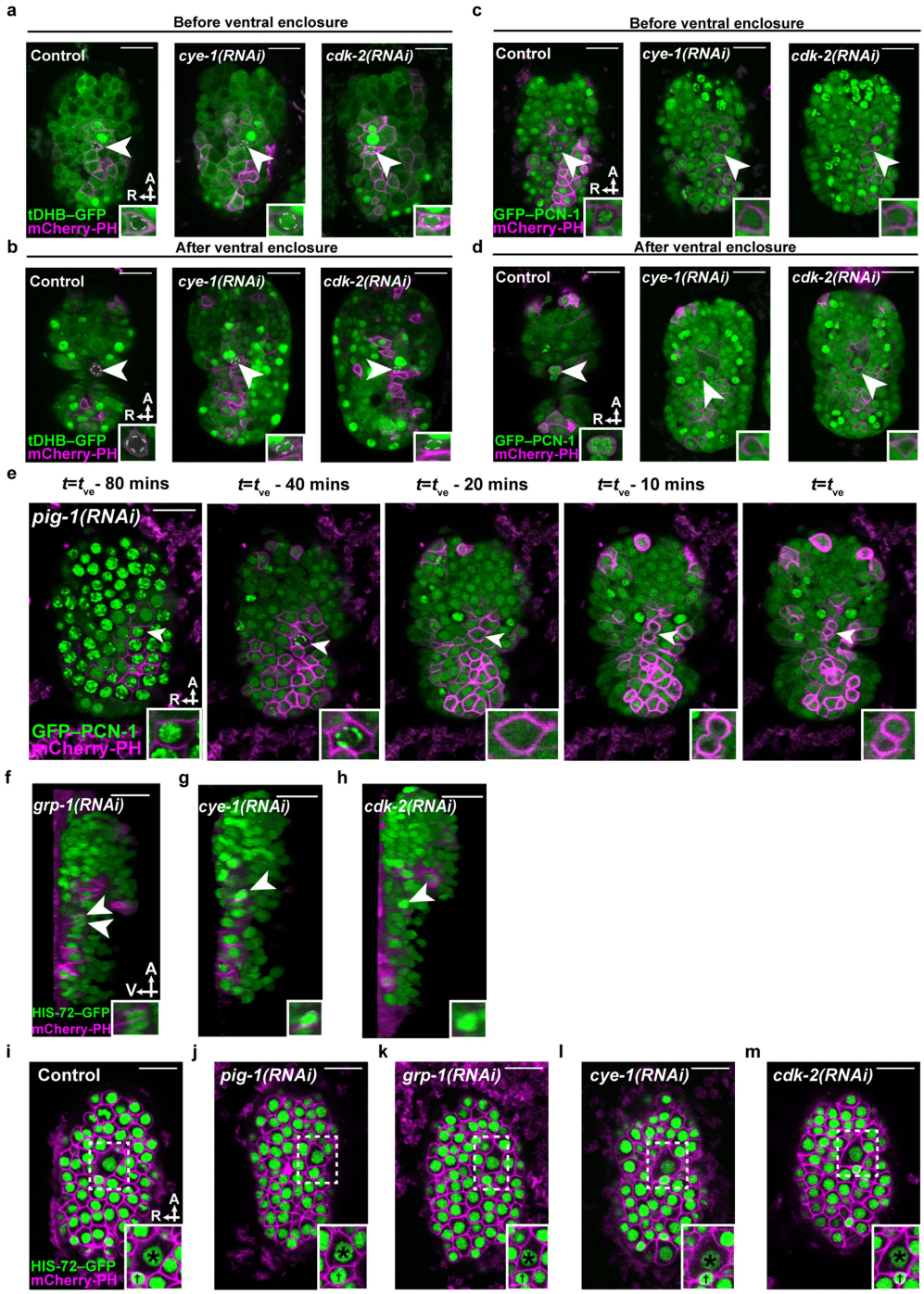


**Extended Data Fig. 3 | ABplpappap, which is generated by an unequal cell division, arrests in S phase and is extruded. a**, **b**, Confocal fluorescence micrographs of tDHB–GFP fluorescence in ABplpappap (arrowheads) before (**a**) and after (**b**) ventral enclosure in *heSi192[$P_{eft\text{-}3}$::tDHB-GFP]; ced-3(lf); nIs861[$P_{egl\text{-}1}$::mCherry::PH]* embryos after the indicated RNAi treatment. Dotted outline, ABplpappap nucleus, as identified by Nomarski optics. **c**, **d**, Confocal fluorescence micrographs of GFP–PCN-1 fluorescence in ABplpappap (arrowheads) before (**c**) and after (**d**) ventral enclosure in *ced-3(lf); isIs17[$P_{pie\text{-}1}$::GFP::pcn-1]; nIs861* embryos after the indicated RNAi treatment. **e**, Time-lapse confocal fluorescence micrographs of GFP–PCN-1 fluorescence in ABplpappap (arrowheads) in a *ced-3(lf); isIs17; nIs861; pig-1(RNAi)* embryo at the indicated times. $t_{ve}$, time point of ventral enclosure. **f**–**h**, Micrographs of virtual lateral section of *ced-3(lf); nIs861; stIs10026* embryos showing either ABplpappap (arrowhead) or its daughter cells (arrowheads) after indicated RNAi treatment. **i**–**m**, Confocal fluorescence micrographs of *ced-3(lf); ltIs44[$P_{pie\text{-}1}$::mCherry::PH]; stIs10026* embryos showing the relative sizes of ABplpappap and its sister cell, ABplpappaa, in embryos after the indicated RNAi treatment. Insets, ABplpappap (**a**–**d**); ABplpappap or its daughters (**e**–**h**); magnified view of the region indicated, which includes ABplpappap (†) and ABplpappaa (*) (**i**–**m**). Scale bars, 10 µm.

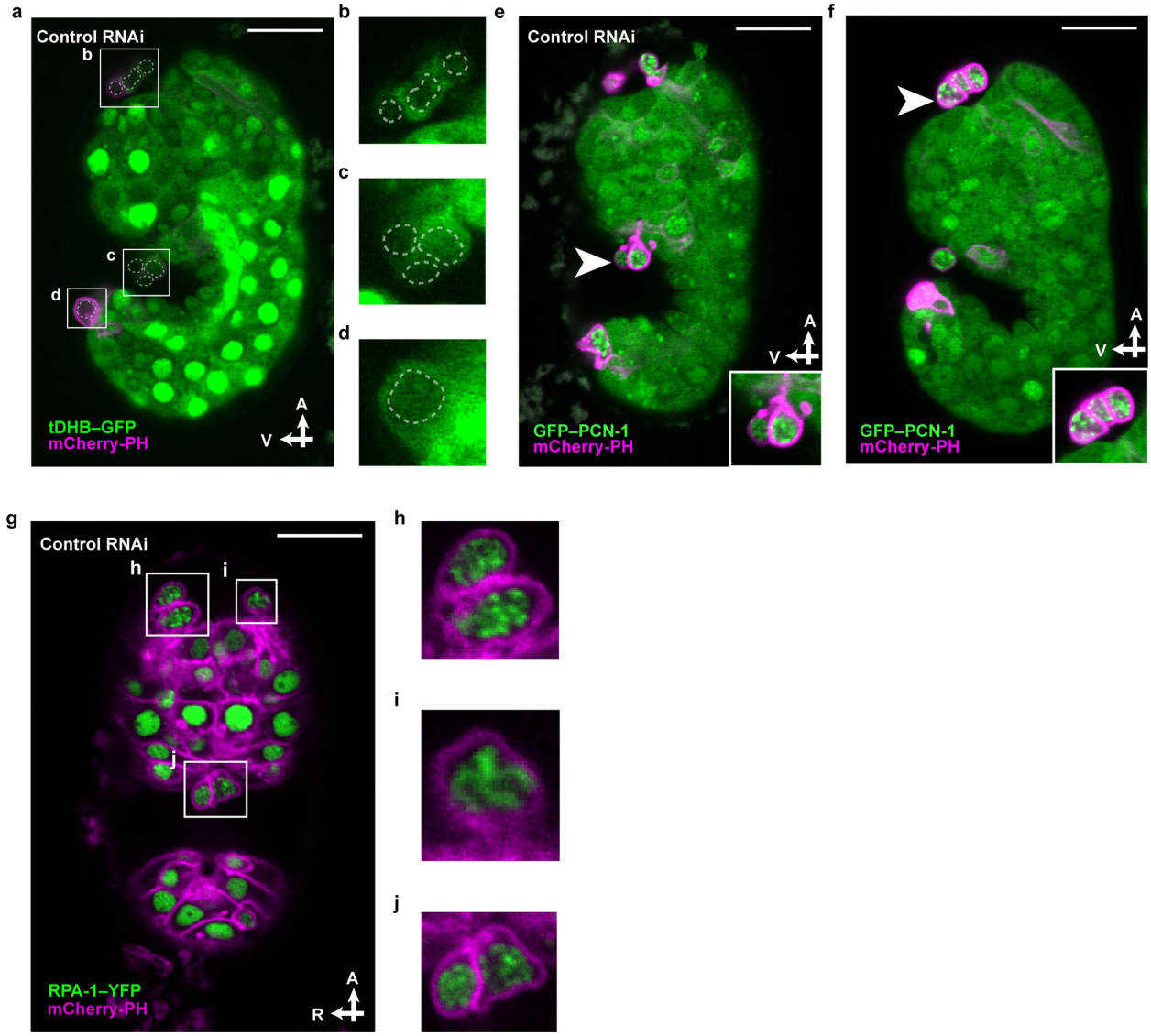


**Extended Data Fig. 4 | All extruded cells display features of cell cycle entry, S-phase arrest, and replication stress. a**–**d**, tDHB–GFP fluorescence in unidentified extruded cells from the anterior sensory depression (**b**), the ventral pocket (**c**), and the posterior tip (**d**) of a comma stage embryo of the genotype *heSi192; ced-3(lf); nIs861* after RNAi against empty vector control. Nuclei of extruded cells, as identified by Nomarski optics, are marked by dotted outlines. **e**, **f**, Micrographs of GFP–PCN-1 fluorescence in unidentified extruded cells (arrowhead) at the ventral pocket (**e**) or the anterior sensory depression (**f**) from *ced-3(lf); isIs17; nIs861* embryos after RNAi against empty vector control (**e**) or no RNAi (**f**). Insets, extruded cells marked by arrowheads in micrographs. **g**–**j**, RPA-1–YFP fluorescence in unidentified extruded cells from the anterior sensory depression (**h**, **i**) and ventral pocket (**j**) in a *ced-3(lf); ltIs44; opIs263[$P_{rpa\text{-}1}$::rpa-1::YFP]* embryo after RNAi against empty vector control. Scale bars, 10 µm.

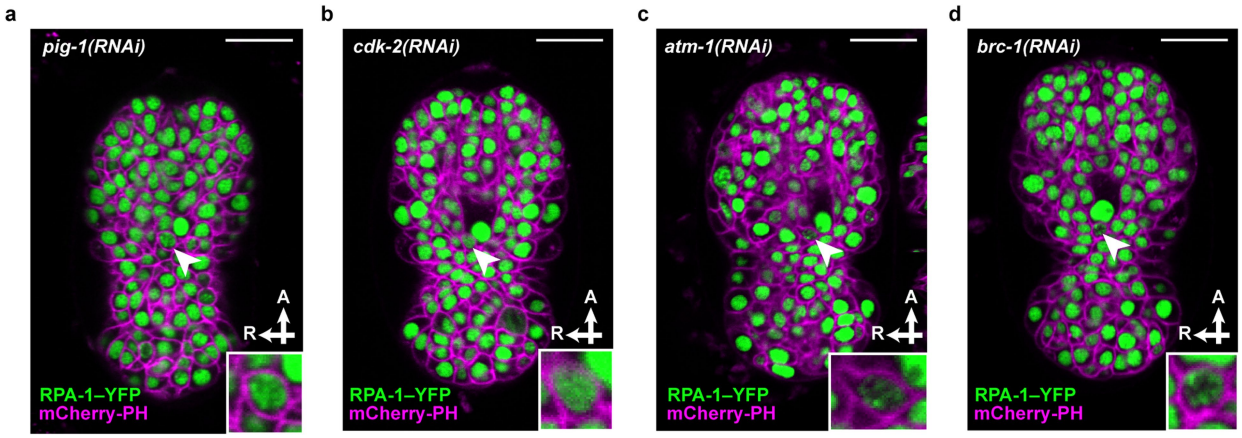


**e**

| Suppressor of *lrr-1(lf)* sterility | Suppressor of *ced-3(lf)* extrusion? |
|---|---|
| *atl-1* | Yes |
| *chk-1* | Yes |
| *mus-101* | Yes |
| *clsp-1* | Yes |
| *psf-2* | Yes |
| *psf-3* | Yes |

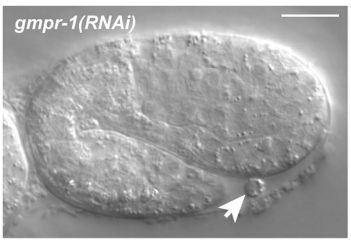


**Extended Data Fig. 5 | The replication-stress response, probably caused by *lrr-1* and nucleotide insufficiency, promotes cell extrusion. a**–**d**, Confocal fluorescence micrographs showing the localization of RPA-1–YFP in ABplpappap (arrowheads) in *ced-3(lf); ltIs44; opIs263* embryos after the indicated RNAi treatment. Insets, magnified views of ABplpappap. **e**, Genes identified as suppressors of the sterility of *lrr-1(lf)* mutants[19] were tested for suppression of cell extrusion. **f**, Nomarski micrograph showing a cell extruded (arrow) from a wild-type embryo after *gmpr-1(RNAi)* treatment. Scale bars, 10 µm.

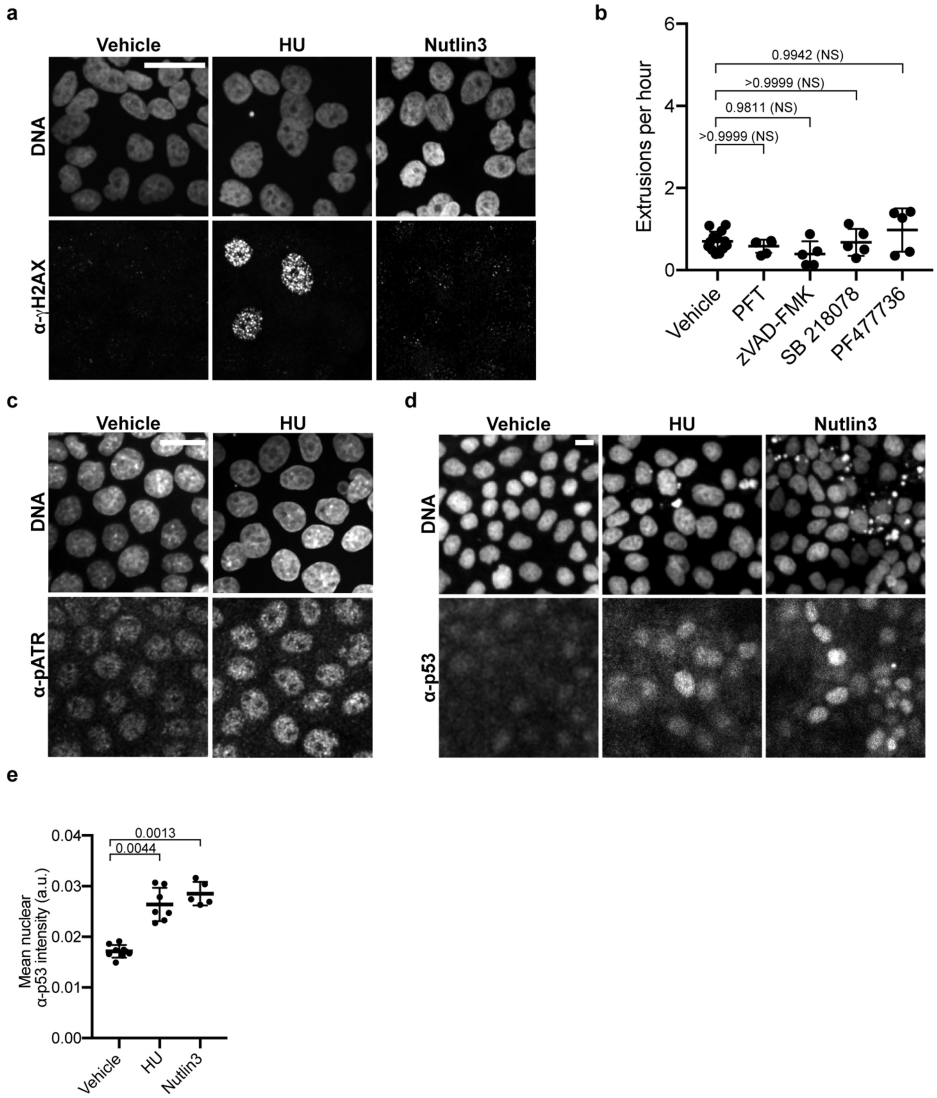


**Extended Data Fig. 6 | Inhibitors of HU-induced replication-stress response and pan-caspase inhibitors do not alter stochastic cell extrusion.** **a**, **c**, **d**, Representative micrographs of anti-γH2AX (**a**), anti-pATR (**c**) and anti-p53 immunofluorescence signal (**d**) in vehicle- or HU-treated MDCK-II cells (**c**), and in vehicle-, HU- or Nutlin3-treated MDCK-II cells (**a**, **d**). DNA is stained with Hoechst. Scale bars, 20 µm. **b**, Quantification of extrusions per hour after the indicated treatments. $n = 13, 6, 5, 5$ and 5 (biological replicates) each for control, PFT, zVAD-FMK, SB 218078 and PF477736 treatments, respectively. Each data point represents a separate experiment. These data were collected and analysed for statistical significance with the data in Fig. 4g. *P* values are indicated; n.s., not significant. **e**, Quantification of anti-p53 immunofluorescence signal in MDCK-II cells treated with vehicle, HU, or Nutlin-3. $n = 9, 7$ and 5 (biological replicates) for vehicle, HU and Nutlin3, respectively. Each data point represents mean fluorescence intensity signal from one image of hundreds of cells. Kruskal–Wallis one-way ANOVA followed by Dunn's correction was performed. *P* values are indicated. Data in **b**, **e** are represented as mean ± s.d.

**Extended Data Table 1 | Penetrances of the Tex phenotype produced by RNAi against cell cycle genes (and non-cell-cycle cyclins and CDKs) in *ced-3(lf)* animals**

| RNAi target | Mammalian Homologue | Percent Tex | n | extensive lethality? |
|---|---|---|---|---|
| empty vector | - | 1 | 159 | N |
| ***atl-1*** | *ATR* | 10 | 509 | N |
| *cdc-14* | *CDC14A/B/C* | 1 | 168 | N |
| *cdc-25.1* | *CDC25A/B/C* | 0 | 111 | Y |
| ***cdc-25.2*** | *CDC25A/B/C* | 12 | 159 | N |
| *cdc-25.3* | *CDC25A/B/C* | 2 | 168 | N |
| *cdc-25.4* | *CDC25A/B/C* | 0 | 183 | N |
| ***cdk-1*** | *CDK1* | 15 | 61 | Y |
| *cdk-11.1* | *CDK11A/B* | 0 | 175 | N |
| *cdk-11.2* | *CDK11A/B* | 1 | 132 | N |
| *cdk-12* | *CDK12* | 0 | 167 | N |
| ***cdk-2*** | *CDK2* | 65 | 181 | N |
| *cdk-4* | *CDK4/6* | 1 | 193 | N |
| *cdk-5* | *CDK5* | 0 | 155 | N |
| *cdk-7* | *CDK7* | 0 | 130 | Y |
| *cdk-8* | *CDK8/19* | 1 | 186 | N |
| *cdk-9* | *CDK9* | 1 | 155 | Y |
| *cdt-1* | *CDT1* | 1 | 147 | Y |
| ***chk-1*** | *CHEK1* | 10 | 164 | Y |
| *cit-1.1* | *CCNT1/2* | 0 | 105 | N |
| *cit-1.2* | *CCNT1/2* | 1 | 244 | N |
| *cki-1* | *CDKN1B* | 0 | 125 | N |
| *cki-2* | *CDKN1A/B/C* | 1 | 216 | N |
| *clk-2* | *TELO2* | 1 | 156 | N |
| *cul-1* | *CUL1* | 5 | 81 | Y |
| *cul-2* | *CUL2* | 0 | 21 | Y |
| *cul-3* | *CUL3* | 5 | 151 | Y |
| *cul-4* | *CUL4* | 0 | 141 | N |
| ***cya-1*** | *CCNA1/2* | 20 | 309 | N |
| *cyb-1* | *CCNB1* | 4 | 136 | N |
| *cyb-2.1* | *CCNB1/2* | 1 | 102 | N |
| *cyb-2.2* | *CCNB1* | 0 | 144 | N |
| *cyb-3* | *CCNB3* | 14 | 7 | Y |
| *cic-1* | *CCNC* | 1 | 158 | N |
| *cyd-1* | *CCND1/2/3* | 0 | 111 | N |
| ***cye-1*** | *CCNE1/2* | 89 | 133 | Y |
| *cyh-1* | *CCNH* | 0 | 119 | Y |
| *cyl-1* | *CCNL1/2* | 1 | 106 | Y |
| *cyy-1* | *CCNY* | 1 | 108 | N |
| *dpl-1* | *TFDP1/2/3* | 0 | 167 | N |
| *efl-1* | *E2F4/5* | 0 | 141 | N |
| *emb-27* | *CDC16* | 0 | 107 | Y |
| *emb-30* | *ANAPC4* | 0 | 130 | Y |
| *fzr-1* | *FZR1* | 1 | 146 | N |
| *fzy-1* | *CDC20* | 0 | 130 | Y |
| *hpr-17* | *RAD17* | 5 | 214 | N |
| *hus-1* | *HUS1/1B* | 0 | 132 | N |
| *lin-15* | - | 1 | 104 | N |
| ***lin-23*** | *BTRC* | 23 | 147 | N |
| *lin-35* | *RB1/RBL1/2* | 0 | 134 | N |
| *lin-36* | - | 0 | 111 | N |
| *lin-9* | *LIN9* | 1 | 125 | N |
| *mat-1* | *CDC27* | 0 | 80 | Y |
| *mat-2* | *ANAPC1* | 1 | 163 | Y |
| *mat-3* | *CDC23* | 0 | 108 | Y |
| *mdf-1* | *MAD1L1* | 3 | 112 | N |
| *mdf-2* | *MAD2L1* | 1 | 111 | N |
| *mrt-2* | *RAD1* | 0 | 114 | N |
| *rnr-1* | *RRM1* | 5 | 103 | Y |
| *san-1* | *BUB1/1B* | 1 | 145 | N |
| *wee-1.1* | *PKMYT1* | 1 | 159 | N |
| *wee-1.3* | *PKMYT1* | 0 | 60 | Y |

Tex penetrance produced by indicated RNAi treatment, mammalian homologue of the RNAi target and whether the RNAi clone produced extensive lethality are shown. Genes corresponding to RNAi clones that produced more than 9% penetrance of the Tex phenotype are in bold. *cyb-3* did not fit this criterion, as extensive lethality prevented the counting of a sufficient number of animals to assign significance. Some cyclins and CDKs that function outside the cell cycle were included and served as negative controls.

**Extended Data Table 2 | Penetrances of the Tex phenotype produced in wild-type animals by RNAi against cell-cycle genes with potential roles in cell extrusion**

| RNAi target | Mammalian Homologue | Percent Tex | n |
|---|---|---|---|
| empty vector | - | 0 | 127 |
| *atl-1* | *ATR* | 0 | 198 |
| *cdc-25.2* | *CDC25A/B/C* | 0 | 36 |
| *cdk-1* | *CDK1* | 0 | 51 |
| *cdk-2* | *CDK2* | 0 | 237 |
| *chk-1* | *CHEK1* | 0 | 115 |
| *csn-1* | *GPS1* | 0 | 156 |
| *csn-4* | *COPS4* | 0 | 141 |
| *csn-5* | *COPS5* | 0 | 114 |
| *cya-1* | *CCNA1/2* | 0 | 167 |
| *cye-1* | *CCNE1/2* | 0 | 143 |
| *lin-23* | *BTRC* | 12 | 96 |
| *psf-1* | *GINS1* | 0 | 150 |
| *psf-2* | *GINS2* | 0 | 190 |
| *psf-3* | *GINS3* | 0 | 72 |

The Tex penetrance produced in wild-type animals by RNAi clones against cell cycle genes that might be involved in cell extrusion (based on the corresponding Tex penetrance in *ced-3(lf)* animals) is provided. Bona fide candidates for cell extrusion regulation should not produce a Tex phenotype in wild-type animals, as cell extrusion does not occur in wild-type embryos. A Tex phenotype in wild-type animals could occur from other effects of RNAi against cell cycle genes, such as excessive proliferation leading to multiple excretory cells. Such proliferation is likely to be the case for *lin-23,* as RNAi against *lin-23* has been previously described to cause excessive proliferation[51]. The 13 other genes are good candidates to be regulators of cell extrusion by the criterion of dependence of the Tex phenotype on the loss of function of *ced-3*.

nature research

Corresponding author(s): H. Robert Horvitz

Last updated by author(s): Mar 27, 2021

# Reporting Summary

Nature Research wishes to improve the reproducibility of the work that we publish. This form provides structure for consistency and transparency in reporting. For further information on Nature Research policies, see our Editorial Policies and the Editorial Policy Checklist.

## Statistics

For all statistical analyses, confirm that the following items are present in the figure legend, table legend, main text, or Methods section.

| n/a | Confirmed | |
|---|---|---|
| ☐ | ☒ | The exact sample size (*n*) for each experimental group/condition, given as a discrete number and unit of measurement |
| ☐ | ☒ | A statement on whether measurements were taken from distinct samples or whether the same sample was measured repeatedly |
| ☐ | ☒ | The statistical test(s) used AND whether they are one- or two-sided<br>*Only common tests should be described solely by name; describe more complex techniques in the Methods section.* |
| ☒ | ☐ | A description of all covariates tested |
| ☐ | ☒ | A description of any assumptions or corrections, such as tests of normality and adjustment for multiple comparisons |
| ☐ | ☒ | A full description of the statistical parameters including central tendency (e.g. means) or other basic estimates (e.g. regression coefficient) AND variation (e.g. standard deviation) or associated estimates of uncertainty (e.g. confidence intervals) |
| ☐ | ☒ | For null hypothesis testing, the test statistic (e.g. *F*, *t*, *r*) with confidence intervals, effect sizes, degrees of freedom and *P* value noted<br>*Give P values as exact values whenever suitable.* |
| ☒ | ☐ | For Bayesian analysis, information on the choice of priors and Markov chain Monte Carlo settings |
| ☒ | ☐ | For hierarchical and complex designs, identification of the appropriate level for tests and full reporting of outcomes |
| ☒ | ☐ | Estimates of effect sizes (e.g. Cohen's *d*, Pearson's *r*), indicating how they were calculated |

*Our web collection on statistics for biologists contains articles on many of the points above.*

## Software and code

Policy information about availability of computer code

| | |
|---|---|
| Data collection | Zen Blue 2.0 was used to obtain time-lapse, z-stack and single micrographs on the confocal microscope and single micrographs on the compound fluorescence microscope. |
| Data analysis | ImageJ 1.52i was used to determine fluorescence signal intensity of C. elegans reporters. Cell Profiler 4.0 and its modules IdentifyPrimaryObjects, MeasureObjectIntensity, and ExportToSpreadsheet were used for nuclear segmentation, nuclear fluorescence intensity measurements, and data export. Mammalian extrusion was quantified with the Cell Counter plugin of Fiji 2.1 distribution of ImageJ 1.53c. Geneious 10.2.6 (Biomatters, Inc.) was used for molecular biology applications, such as cloning and verification of RNAi clone sequences by alignment to target genes. Photoshop CC 2019 and Illustrator CC 2019 (Adobe) were used for preparing images for final publication. The Time Stamper function in the Stowers ImageJ plugin was used to mark elapsed time on time-lapse videos. GraphPad Prism 7.0 was used to perform all statistical analysis and graph generation. |

For manuscripts utilizing custom algorithms or software that are central to the research but not yet described in published literature, software must be made available to editors and reviewers. We strongly encourage code deposition in a community repository (e.g. GitHub). See the Nature Research guidelines for submitting code & software for further information.

## Data

Policy information about availability of data

All manuscripts must include a data availability statement. This statement should provide the following information, where applicable:

- Accession codes, unique identifiers, or web links for publicly available datasets
- A list of figures that have associated raw data
- A description of any restrictions on data availability

Data supporting all figures are available within this paper and in the associated source data files. Raw microscopy data are available upon request to the corresponding author.

# Field-specific reporting

Please select the one below that is the best fit for your research. If you are not sure, read the appropriate sections before making your selection.

☒ Life sciences ☐ Behavioural & social sciences ☐ Ecological, evolutionary & environmental sciences

For a reference copy of the document with all sections, see nature.com/documents/nr-reporting-summary-flat.pdf

# Life sciences study design

All studies must disclose on these points even when the disclosure is negative.

| | |
|---|---|
| Sample size | No statistical methods were used to predetermine sample size. For quantification of the penetrance of the Tex phenotype in Caenorhabditis elegans, at least 100 animals were scored unless extensive lethality occurred as a result of RNAi treatment. For analysis of cell extrusion from RNAi-treated live C. elegans embryos we found that 5 to 10 randomly selected embryos largely reflected the penetrance of Tex phenotype observed in animals in which ABplpappap either did not enter the cell cycle or completed the cell cycle. We therefore used 5 to 10 C. elegans embryos for all such analyses. For genetic mosaic analysis, we examined 10 larval animals, and the result from all 10 animals led to the same conclusion. For mammalian cell culture experiments, each experimental run yielded hundreds (live) or thousands (stainings) of cells to analyze, and statistical comparisons were robust for each run. |
| Data exclusions | No data were excluded from analysis. |
| Replication | All experiments using C. elegans animals were performed at least three times and successfully replicated each time. Similarly, findings from live mammalian cell extrusion and nuclear stainings were successfully replicated at least three times. |
| Randomization | C. elegans larval animals and embryos and mammalian cells were randomly chosen for imaging and quantification for each condition in each experiment. |
| Blinding | The investigators were blinded to the identity of individual RNAi clones during the genome-wide RNAi screen. Experiments requiring imaging of C. elegans embryos could not be effectively blinded, as RNAi treatments produced developmental phenotypes that made the identity of the target gene obvious. For live imaging of mammalian cell extrusion the number of cell extrusions per XY position was quantified without knowing the corresponding treatment. Mammalian cell staining analysis was automated , reducing the risk of human-originated bias |

# Reporting for specific materials, systems and methods

We require information from authors about some types of materials, experimental systems and methods used in many studies. Here, indicate whether each material, system or method listed is relevant to your study. If you are not sure if a list item applies to your research, read the appropriate section before selecting a response.

### Materials & experimental systems

| n/a | Involved in the study |
|---|---|
| ☐ | ☒ Antibodies |
| ☐ | ☒ Eukaryotic cell lines |
| ☒ | ☐ Palaeontology and archaeology |
| ☐ | ☒ Animals and other organisms |
| ☒ | ☐ Human research participants |
| ☒ | ☐ Clinical data |
| ☒ | ☐ Dual use research of concern |

### Methods

| n/a | Involved in the study |
|---|---|
| ☒ | ☐ ChIP-seq |
| ☒ | ☐ Flow cytometry |
| ☒ | ☐ MRI-based neuroimaging |

## Antibodies

| | |
|---|---|
| Antibodies used | Primaries (overnight, 4ºC):<br>- p53, Abcam cat# ab26, clone PAb 240, lot GR3318620-1, used 1:250 in PBS |

- phospho-ATR (Ser248), ThermoFisher cat# 720107, polyclonal, lot RF238543, used 1:250 in PBS
- phospho-histone H2A.X (Ser139), CellSignaling cat# 9718, clone 20E3, lot 17m, used 1:250 in PBS

Secondaries (1h, room temperature):
- Goat anti-Rabbit IgG (H+L) Cross-Adsorbed Secondary Antibody, Alexa Fluor 488, ThermoFisher cat# A-11008, polyclonal, lot unknown, used 1:250 in PBS.
- Goat anti-Mouse IgG (H+L) Cross-Adsorbed Secondary Antibody, Alexa Fluor 594, ThermoFisher cat# A-11005, polyclonal, lot unknown, used 1:250 in PBS.

Alexa 647 Phalloidin, Thermofisher, cat#A22287, unknown lot, used 1:500 in PBS
Hoechst, Thermofisher, cat# 62249, unknown lot, used 30 ug/mL in PBS

Validation

anti-p53: KO validated, reacts with dog, suitable for IF experiments (https://www.abcam.com/p53-antibody-pab-240-ab26.html)
- anti-phosphoATR is validated by hydroxyurea treatment and immunostaining. (https://www.thermofisher.com/antibody/product/Phospho-ATR-Ser428-Antibody-Polyclonal/720107)
- anti phospho-histone H2A.X works for immunostaining cells treated with hydroxyurea. (https://www.cellsignal.co.uk/products/primary-antibodies/phospho-histone-h2a-x-ser139-20e3-rabbit-mab/9718)

Our experiments compared control conditions to hydroxyurea (HU) treatments, known to up-regulate, among others, our proteins of interest p53, pATR, and pH2AX. Remarkably, HU is used as positive control in several antibody verification immunostaining experiments, according to the manufacturers websites. Our results in dog cells match the responses in previous studies in other species, i.e. an increase in the nuclear signal of the three target proteins only seen in HU-treated cells, not control counterparts.

## Eukaryotic cell lines

Policy information about cell lines

Cell line source(s)

- MDCK-II: European Collection of Authenticated Cell Cultures (ECACC) operated by Public Health England, catalogue number 00062107, lot 19G037.
- MDCK-Fucci: gift from Xavier Trepat lab, generated at the L.Hufnagel lab.

Authentication

- MDCK-II: ECACC cell lines authenticated before shipping. Cells were not authenticated after reception.
- MDCK-Fucci: not authenticated

Mycoplasma contamination

Cell lines tested for Mycoplasma contamination before shipping. Cells were not tested after reception.

Commonly misidentified lines
(See ICLAC register)

None

## Animals and other organisms

Policy information about studies involving animals; ARRIVE guidelines recommended for reporting animal research

Laboratory animals

Caenorhabditis elegans strains used:
N2 (Wild-type strain)
MT4434 ced-5(n1812) IV
MT12054 ced-3(n3692) IV
MT20083 nIs433 I
MT20084 nIs434 X
MT20117 nIs433 I; ced-3(n3692) IV
MT20131 ced-3(n3692) IV; nIs434 X
MT26340 cye-1(eh10)/hT2[qIs48] I; hT2[qIs48]/+ III; nIs434 X
MT26342 cye-1(eh10)/hT2[qIs48] I; hT2[qIs48]/+ III; ced-3(n3692) IV; nIs434 X
MT26360 cye-1(eh10)/hT2[qIs48] I; hT2[qIs48]/+ III; ced-3(n3692) IV; nIs434 X; nEx3043
MT22450 ced-3(n3692) IV; stIs10026; nIs632
MT25639 ced-3(n3692) IV; stIs10026; nIs861
MT25640 heSi192 II; ced-3(n3692) IV; nIs861
MT25692 ced-3(n3692) IV; ltIs44 V; stIs10026
MT25807 ced-3(n3692) IV; nIs861; isIs17
MT26335 ced-3(n3692) IV; ltIs44 V; opIs263
MT25640, MT25692, MT25807 and MT26335 might be carrying the unc-119(ed3) mutation in the background, which is rescued by a the transgenes heSi192, ltIs44, isIs17 and ltIs44 in these strains, respectively.

Wild animals

Study did not involve animals caught in the wild.

Field-collected samples

Study did not involve samples collected from the field.

Ethics oversight

No ethical approval or guidance was required, as such approval or guidance is not required for work with Caenorhabditis elegans.

Note that full information on the approval of the study protocol must also be provided in the manuscript.